DUAL CIRCULARLY POLARIZED HORN ANTENNA AND FEED NETWORK FOR FULL KA-BAND SATCOM

ŞEVVAL OKSAY

ÖZYEĞİN UNIVERSITY

JANUARY, 2026

DUAL CIRCULARLY POLARIZED HORN ANTENNA AND FEED NETWORK FOR FULL KA-BAND SATCOM

by
Şevval Oksay

Thesis
Submitted in Partial Fulfillment of the
Requirements for the Degree of

Master of Science

in
Electrical and Electronics Engineering

Advisor: Asst. Prof. Ahmed H. Akgiray

Graduate School of Science and Engineering
Özyeğin University
İstanbul

January, 2026

DUAL CIRCULARLY POLARIZED HORN ANTENNA AND FEED NETWORK FOR FULL KA-BAND SATCOM

Approved by:

Asst. Prof. Ahmed H. Akgiray, Advisor
Department of Electrical and Electronics Engineering
Özyeğin University

Asst. Prof. Göktürk Poyrazoğlu
Department of Electrical and Electronics Engineering
Özyeğin University

Asst. Prof. Onur Hamza Karabey
Institute of Defence Technologies
Gebze Technical University

Approval Date: Dec 16, 2025

To my family

DECLARATION OF ORIGINALITY

I hereby declare that I am the sole author of this thesis and that this is the true copy of my thesis, including the final revisions, approved by my thesis committee. All data and information have been obtained, produced, and presented in accordance with the rules of research ethics and principles of academic honesty. As required by these rules, to the best of my knowledge I have acknowledged ideas, thoughts, and any copyrighted material in accordance with the standard referencing rules. I certify that any part of this thesis has not been submitted for a degree or diploma in another educational institution.

Şevval Oksay

ABSTRACT

A compact, dual circularly polarized corrugated horn antenna and feed network system designed for small GEO satellites is presented in this thesis. The system covers the entire SATCOM Ka-band, including military frequencies from 17.7-21.2 GHz and 27.5-31 GHz. The structure comprises two main sections: the antenna section, which includes a corrugated horn antenna and a radial mode converter, and the feed network, which contains a circular-to-square waveguide transition, a six-port ortho-mode junction, waveguide low-pass filters, H-plane bends, a five-port ortho-mode junction, septum polarizers, and adapters. The transmitter frequency band is 17.7-21.2 GHz, and the receiver frequency band is 27.5-31 GHz. The minimum and maximum gains are 21.1 dBi and 23.9 dBi for the transmitter, and 23.8 dBi and 26.5 dBi for the receiver, respectively. The sidelobe level is below -31.3 dBc, and the polarization is circular. The cross-polarization discrimination exceeds 30 dB for both bands. Port-to-port isolation surpasses 20 dB, Tx-Rx isolation is greater than 63 dB, and return loss is above 30 dB. The interface uses WR51 standard waveguide at transmitter and WR34 standard waveguide at receiver. The overall structure is less than 110 x 110 x 360 mm^3. The radiation patterns of both the corrugated horn antenna and the overall system are discussed as well.

Keywords: Corrugated horn antenna, dual circular polarization, feed network, ortho-mode junction, waveguide

ÖZET

Bu tezde, küçük GEO uyduları için tasarlanmış kompakt, çift dairesel polarizasyonlu dişli boynuz anteni ve besleme ağı sistemi sunulmaktadır. Sistem, 17.7-21.2 GHz ve 27.5-31 GHz askeri frekanslarını da içeren tüm SATCOM Ka-bandını kapsamaktadır. Yapı iki ana kısımdan oluşmaktadır: dişli boynuz anten ve radyal mod dönüştürücüsünü içeren anten bölümü ile daireselden kare dalga kılavuzu geçiş, altı çıkışlı ortogonal mod birleştirici, dalga kılavuzu alçak geçiren filtreleri, H-düzlemi kıvrımları, beş çıkışlı ortogonal mod birleştirici, septum kutuplaştırıcılar ve adaptörleri içeren besleme ağı bölümü. Verici frekans bandı 17.7-21.2 GHz, alıcı frekans bandı ise 27.5-31 GHz'dir. Verici için minimum ve maksimum kazanç sırasıyla 21.1 dBi ve 23.9 dBi; alıcı için ise 23.8 dBi ve 26.5 dBi'dir. Yan lob seviyesi -31.3 dBc'nin altındadır ve polarizasyon daireseldir. Her iki bant için çapraz polarizasyon ayrımı 30 dB'yi aşmaktadır. Portlar arası izolasyon 20 dB'nin üzerindedir. Arayüzü, vericide WR51 ve alıcıda WR34 standart dalga kılavuzunu kullanır. Yapının toplam boyutları 110 x 110 x 360 mm^3'ten küçüktür. Hem dişli boynuz antenin hem de tüm yapının ışıma örüntüleri de tartışılmaktadır.

Anahtar Kelimeler: Dişli boynuz anten, çift dairesel polarizasyon, besleme ağı, ortogonal mod birleştirici, dalga kılavuzu

ACKNOWLEDGEMENTS

This work was partially supported by CTECH BİLİŞİM TEKNOLOJİLERİ SAN. VE TİC. A.Ş.

I would like to express my gratitude to my thesis advisor, Asst. Prof. Ahmed H. Akgiray, for his contribution to the completion of this work.

I am deeply grateful to my parents for their unwavering support, for encouraging me in every situation, and for guiding me to become an honest individual, inspired by the values inherent in the engineering profession.

Finally, I sincerely thank my closest friend, Simge Ece Erer, who has supported and encouraged me in many ways since the first days of my undergraduate studies.

TABLE OF CONTENTS

LIST OF TABLES

LIST OF FIGURES

LIST OF SYMBOLS

f_c	: Center frequency
f_o	: Output frequency
f_{min}	: Minimum frequency
f_{max}	: Maximum frequency
λ_c	: Wavelength corresponding to the center frequency
k_c	: Wavenumber corresponding to the center frequency
λ_o	: Wavelength corresponding to the output frequency
k_o	: Wavenumber corresponding to the output frequency
L	: Length
N_{hr}	: Number of slots
$a_{i,hr}$	: Input radius of the horn
$a_{o,hr}$	: Output radius of the horn
$a_{j,hr}$	: Radius at a point along the horn
$a_{i,mc}$	: Input radius of the mode converter
$a_{o,mc}$	: Output radius of the mode converter
$a_{j,mc}$	: Radius at a point along the mode converter
K	: Correction Factor
$d_{j,hr}$	: Depth of the jth slot of the horn
$d_{j,mc}$	: Depth of the jth slot of the mode converter
σ_{MC}	: Percentage factor for the first slot depth of the mode converter

LIST OF ACRONYMS AND ABBREVIATIONS

CAD	Computer-Aided Design
FD	Frequency Domain
EOC	Edge of Coverage
GEO	Geostationary Earth Orbit
LHCP	Left-hand Circular Polarization
MATLAB	Matrix Laboratory
OMJ	Ortho-mode Junction
OMT	Ortho-mode Transducer
RF	Radio Frequency
Rx	Receiver
RHCP	Right-hand Circular Polarization
SATCOM	Satellite Communication
TD	Time Domain
TEM	Transverse Electromagnetic
Tx	Transmitter
XPD	Cross-polarization Discrimination

1. INTRODUCTION

As technology develops year by year to respond to people's needs, one remarkable improvement is the enhancement of globalization of communication. Hence, efforts in this field of research have been expedited to facilitate global communication services. Satellites contribute to achieving the optimal performance level in communication services more efficiently. Owing to its wide coverage, Satellite Communication (SATCOM) considerably expands connectivity by adapting to varied environments and conditions [1, 2]. Small Geostationary Earth Orbit (GEO) satellites are consistently employed in satellite communications. They orbit the Earth at high speed and are designed to ensure wide coverage. These systems deliver high performance by integrating compact design, low cost, and flexibility [3]. As a result, antennas are specifically designed for use on small GEO satellites are being implemented to provide efficient and reliable communication. In SATCOM applications, antenna technologies have improved to comprise a design capable of operating across different frequency ranges and polarization types. With these features, it allows people to have more robust and accelerated communication.

Several key factors to examine when designing a SATCOM antenna comprise the frequency bands used, gain, polarization diversity, and footprint of the antenna. The most commonly employed frequency band in SATCOM technologies/applications is the Ka-band, as it allows communication across a broad bandwidth [4]. Circular polarization is used in Ka-band SATCOM to accommodate different atmospheric conditions and minimize polarization losses.

A dual-band antenna system can operate both as a Tx and a Rx. In dual circular polarization, two orthogonally polarized channels, namely Left-hand Circular Polarization (LHCP) and Right-hand Circular Polarization (RHCP), are used to minimize cross-polarization interference [5]. Hence, the signal can be transmitted and received simultaneously.

Designing a SATCOM antenna system with both dual-band and dual circular polarization characteristics requires a complex design process. The system comprises a corrugated horn antenna, a radial mode converter, and a feed network in order to provide satellite communication. The corrugated horn antenna is employed because it enables circular polarization, low signal loss, low sidelobe levels, and high gain [6]. Circular polarization is crucial because it enables the exchange of the signal without high loss. A low sidelobe level in the radiation pattern is significant because it reinforces the main beam and reduces any undesired signal leakage into the sidelobes [5]. Another essential component employed in SATCOM is a radial mode converter. This component is used because it ensures that the desired performance is fulfilled from the corrugated horn antenna. Another target is to allow mode conversion with reduced loss. Finally, the feed network is one of the most significant components. It is designed to minimize the signal loss and ensure high-purity circular polarization.

To achieve these objectives, a compact horn antenna and feed network with dual circular polarization for Ka-band SATCOM employed in small GEO satellites are selected for this thesis. A corrugated horn antenna and the radial mode converter are selected because they are widely employed in SATCOM. Since dual-band operation is required, all components are designed to provide Radio Frequency (RF) performance within the Ka-band for both Tx and Rx. For this purpose, a bandwidth of 17.7-21.2 GHz in the Tx band and 27.5-31 GHz in the Rx band is chosen, which ensures wide operating ranges for the extended Ka-band. Using the designed components, the desired LHCP and RHCP are achieved.

In the literature, various studies exist both on antenna systems and on the components that comprise the feed network. These studies describe differences in terms of operating frequency ranges, RF performance, and structural design. Comparisons with these studies exhibit the necessity of the design proposed in this thesis. Based on this information, the Introduction is organized into two sections: Section 1.1 reviews the literature, and Section 1.2 introduces the design approaches used in this work.

1.1 Literature Review

In a previous study, similar antenna and feed network structures have been designed and employed to achieve specific application requirements. In this work, the feed network, which operates in dual polarization with a Rx band of 17.7-21.2 GHz and a Tx band of 27.5-31 GHz, includes low-pass filters, an Ortho-mode Junction (OMJ), a turnstile power divider, septum polarizers for two frequency bands, and a corrugated horn antenna [7]. The feed network exhibits a return loss higher than 20 dB, a Tx - Rx isolation exceeding 85 dB, and the port isolations greater than 18 dB. With the integration of the corrugated horn antenna into the system, the return loss increases to values over 30 dB, and the Tx - Rx isolation improves above 100 dB. Moreover, the six-port OMJ is designed using both circular and rectangular waveguides. Rectangular waveguides of different dimensions are integrated for the arms of the six-port OMJ, with their dimensions designed based on the specified cutoff frequencies to promote operation in the desired waveguide modes.

Whereas the OMJ and Ortho-mode Transducer (OMT) functions are based on similar operating principles, they have some differences in structural design and employment. In high-capacity transceiver systems using dual polarization, the OMT is a crucial component of the antenna-feed network system. Park et al. [8] investigate an OMT operating in the 9.2-12.4 GHz frequency range, and it includes a turnstile junction and E-plane T-shaped power combiners. The compact size of this design ensures a benefit in terms of implementation. The return loss exceeds 18.5 dB, and the cross-polarization is above 35 dB.

In another study, a circular waveguide is utilized for the high-frequency band, while rectangular waveguides are employed for the low-frequency band within the same six-port OMT topology, operating with downlink frequencies of 3.4-4.8 GHz and uplink frequencies of 5.85-7.025 GHz, exceeding 17 dB at the common port and supporting dual linear polarization [9]. This structure is implemented as a linear profile slot-coupled OMT for signal distribution purposes. Especially, no blend is applied to the rectangular waveguides in that design.

In another fabricated feed network, the system operates in 19.25-20.75 GHz and 27-29 GHz [10]. In this design, both the six-port OMJ and five-port OMJ are completely composed of circular waveguides. The measured results acquired from the fabricated prototype closely match the simulated results. After fabrication, measurements show return loss better than 28 dB and port-to-port isolation exceeding 19 dB in terms of polarization. Moreover, this structure represents the first demonstration of a fully monolithically additive-manufactured antenna feed network operating in these frequency ranges.

The European Space Agency's ESA ARTES-4 program designs and fabricates the OMT to operate in C-band, with the antenna interface section implemented using a circular waveguide. The simulation results of this system closely correspond to the measurement results. Return loss is better than 26 dB for each port, while the port-to-port isolation exceeds 23 dB, and the cross-polarization discrimination is greater than 30 dB [11].

A system that includes a horn, Tx/Rx polarizer network, and OMJ comprising a diplexer, operates with a transmit frequency range of 17.7-20.2 GHz and a receive frequency range of 27.5-30 GHz [12]. Comparison between simulation and measurement results show that the design employs dual circular polarization and achieves above 25 dB return loss and greater than 21 dB port-to-port isolation across both frequency bands.

Septum polarizers are typically initiated with a step design; nonetheless, through optimization, the number of steps can be decreased without compromising performance

[13]. These steps play a critical role in achieving the required polarization conversion by accurately controlling both the magnitude and phase difference of the propagating signal, consequently, minimizing potential polarization errors. The component is designed to feed square waveguides for easy integration with the OMJ and to develop high-purity right-hand or left-hand circular polarization. During the number of steps modification procedure, adjustments are made according to the dimensions of the OMJ to provide compatibility and optimal performance.

Gong et al. [14] design a system that includes a corrugated horn antenna, an OMJ, K/Ka band polarizers, low-pass filters, waveguides, and a turnstile junction. In this antenna-feed model, the Tx operates in the 17.7-20.2 GHz and the Rx in the 27.5-30 GHz. It is designed to generate dual circular polarization. Return loss is above 30 dB for both frequency bands, and the port-to-port isolation exceeds 19 dB. The wideband dual circular polarization and frequency ranges provide good RF performance, enabling its employment in satellite services.

1.2 Design Perspectives

To make communication more accessible in small GEO satellites, a structure comprising two main sections, antenna and feed network, is designed for the specified operating frequency with dual circular polarization on the satellite side of a SATCOM link. Due to the dual-band design, this overall system allows the operation in both Tx and Rx bands simultaneously with a compact footprint [15]. For the purpose of enhancing the entire system performance, a dual-diversity approach, namely combining polarization and frequency, has been implemented, therefore increasing the efficiency of the whole system and seamless signal transmission across the Tx and Rx bands. The integrated system covers the entire SATCOM Ka-band, including the military frequency ranges of 17.7-21.2 GHz and 27.5-31 GHz [4, 16]. The reason for selecting the extended Ka-band in this design is to provide a wide bandwidth, compatibility with compact antennas, and high capacity [17].

The antenna consists of a corrugated horn antenna and a radial mode converter. The feed network consists of a circular-to-square waveguide transition, a six-port OMJ, waveguide low-pass filters, H-plane bends, a five-port OMJ, septum polarizers, and adapters. The integrated antenna-feed model is symmetric, and each component is first designed as a vacuum model and then converted to aluminum, with blends and radii applied. Table 1.1 presents the specifications of this antenna-feed network system design. The dimension of the integrated system is less than 160 x 160 x 450 mm³.

Table 1.1: *Design Specifications.*

Parameter	**Transmit**	**Receive**
Operating Frequency	17.7-21.2 GHz	27.5-31 GHz
Polarization	RHCP & LHCP	RHCP & LHCP
Minimum Gain	21 dBi	23.3 dBi
Maximum Gain	23.3 dBi	26.8 dBi
Sidelobe Level	< -30 dBc @ $\lvert\theta\rvert > 30°$	< -30 dBc @ $\lvert\theta\rvert > 30°$
Cross-Polarization Discrimination	$\geq$ 30 dB over Edge of Coverage (EOC)	$\geq$ 30 dB over EOC
Return Loss	$>$ 30 dB (for each port)	$>$ 30 dB (for each port)
Port-to-port Isolation	$>$ 20 dB (over EOC)	$>$ 20 dB (over EOC)
Tx-Rx Isolation	$>$ 80 dB	$>$ 80 dB

In this thesis, a compact, dual circularly polarized corrugated horn antenna and feed network system designed for small GEO satellites, covering the full SATCOM Ka-band, is presented. With this thesis, design methodology covering the integrated design of the antenna section and feed network section, radiation pattern results of this system, and critical performance metrics such as return loss, port-to-port isolation, Tx-Rx isolation, sidelobe level, and cross-polarization discrimination are also discussed. Each structure in this thesis is designed using CST Studio Suite.

In summary, as can be indicated from the examples in the previously mentioned literature, research on this ongoing topic has been conducted from the past to the present and advances. With the advancement of technology, particularly satellite communication, the opportunities offered to people in the field of communication are steadily growing. This thesis aims to contribute to this research field by advancing existing designs, even though similar structures are present, this design has been optimized through fabrication feedback, leading to a state-of-the-art approach in terms of performance and the designed system.

This thesis comprises four chapters. In the second chapter, the design of the antenna and feed network is provided. Each component in the two main sections is examined based on its structure, and the corresponding graphs are analyzed for the performance of the components. Chapter 3 introduces the results of the integrated system. The antenna-feed model is explained in detail, and subsequently, the corresponding graphs are interpreted. In the final chapter, the overall system discussed throughout the thesis is summarized in detail.

2. DESIGN OF THE ANTENNA AND FEED NETWORK

The design and simulation results of each component comprising the system are explained in detail in this chapter. A block diagram of the complete feed and corrugated horn system is presented in Figure 2.1. The signal operating in the Rx band first propagates through the corrugated horn antenna, then travels through the circular-to-square waveguide transition. Subsequently, the Rx signal proceeds to travel through the six-port OMJ via a rectangular waveguide and arrives at the Rx septum polarizer. The dual-polarized signal at the output of the septum polarizer is transmitted to the feed network input/output interface through symmetric adapters designed in WR34 standard waveguide dimensions.

The transmit signal propagating through the WR51 standard waveguide is guided through the low-band septum polarizer. This signal is symmetrically divided into four arms of the five-port OMJ. Each of these arms comprises H-plane bends followed by waveguide low-pass filters implemented in two different structural configurations. The filtered signals are subsequently recombined at the six-port OMJ. Finally, the combined signals pass through the circular-to-square waveguide transition and afterward reach the corrugated horn antenna.

All elements of the system are designed separately in commercial electromagnetic simulation software CST Studio Suite. In addition, custom scripts developed in Matrix Laboratory (MATLAB), Python, and Excel are used to design the system.

The overall system is symmetric, and each component is first designed as a vacuum model and subsequently converted to aluminum, with blends and radii applied. All components, excluding the corrugated horn antenna, are simulated using the Frequency Domain (FD) solver, whereas the antenna itself is examined using the Time Domain (TD) solver.

Accuracy and iterative convergence of the simulation results in all components are confirmed through extensive mesh enhancement trials and solver settings variations. Adaptive mesh enhancement is enabled for all structures except the corrugated horn antenna to ensure computational convergence and solution accuracy.

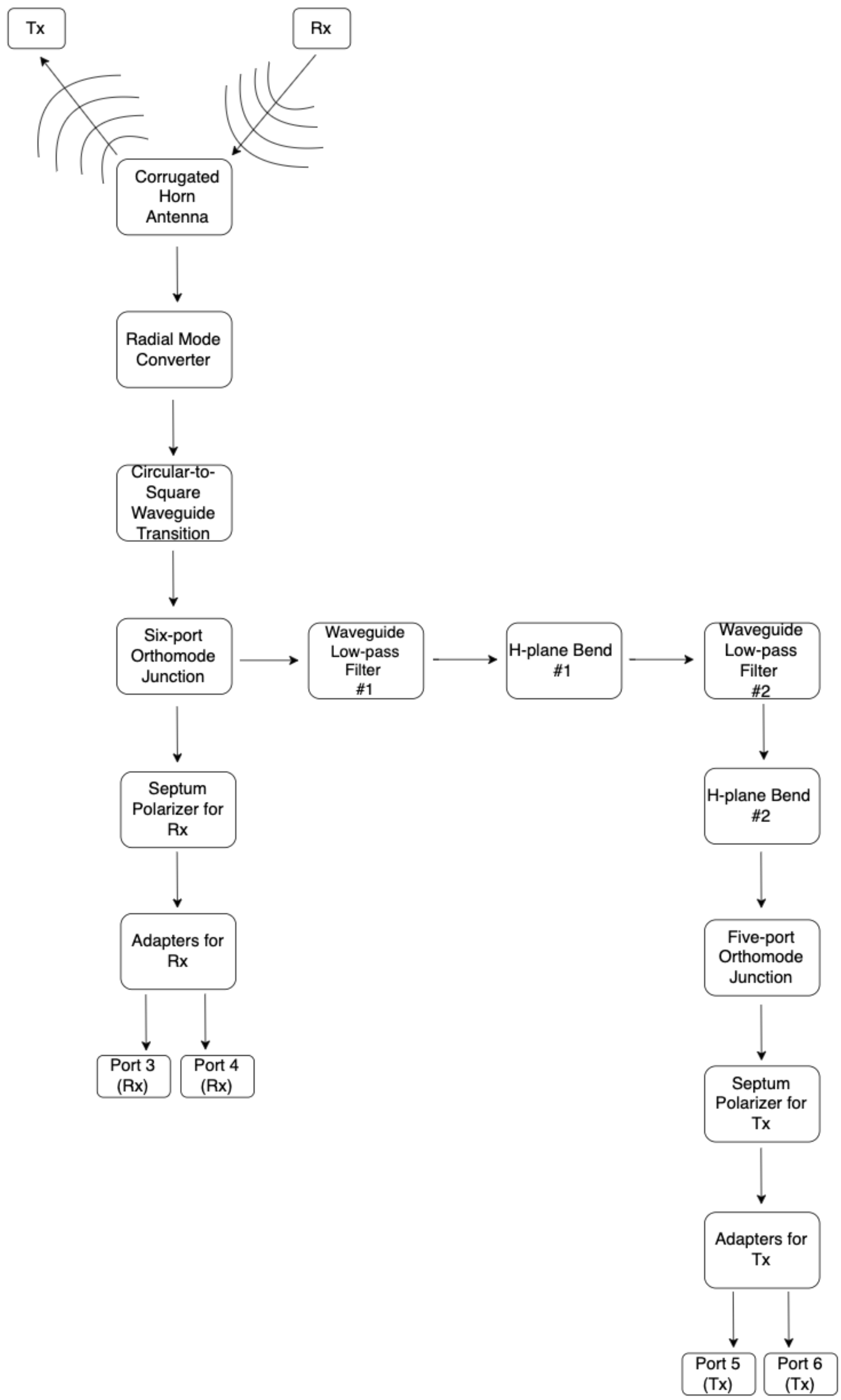

Figure 2.1: *Block Diagram of the Integrated System.*

2.1 Corrugated Horn Antenna

Hybrid-mode corrugated horns are employed as signal feeding for reflector antennas. Radiation patterns obtained with hybrid modes exhibit low cross polarization, excellent radiation symmetry, and low sidelobe levels [6, 18]. The input of the corrugated horn antenna is a circular waveguide, where the fundamental TE_{11} mode at the waveguide input is transformed into the HE_{11} mode within the mode converter.

It is challenging to finalize the design of the mode converter separately from the corrugated horn antenna, because the mode converter performance depends on the mode impedances presented by the corrugated horn antenna, which differ from those provided by the waveguide ports employed in the simulation. In this design, the mode converter and the corrugated horn antenna are first designed individually to reach a reasonable performance level. Afterwards, the components are integrated, and optimization is carried out on the integrated mode converter and corrugated horn.

The need for using the HE_{11} mode arises from the fact that TE_{11} mode alone is inadequate for the efficient operation of such a structure. When only the TE_{11} mode is present, increased cross-polarization and sidelobe levels are examined, rendering it insufficient as an efficient feed. To obtain a Gaussian-like main beam with low cross-polarization and sidelobe levels, a field distribution similar to the Transverse Electromagnetic (TEM) mode, which does not exist in metallic waveguides, is aimed for. For this reason, the HE_{11} mode is efficiently employed [6, 18, 19].

To mitigate the field distortions generated by the TE_{11} mode alone, a TM_{11} mode component is introduced. Owing to the corrugated structure, the TE_{11} and TM_{11} modes enable to propagate with the identical phase velocities, allowing the hybrid-mode composition to be preserved without degradation. An 85% TE_{11} and 15% TM_{11} modal ratio emerges as the optimal solution dictated by the boundary conditions, desired far-field characteristics, Maxwell's equations [6, 18, 19].

The TE_{11} mode exhibits a pronounced radial electric field near the waveguide wall, which gives rise to unwanted effects. In contrast, the TM_{11} mode contributes only weakly in the central region while generating a radial field of opposite polarity close to the wall. Adding a TM_{11} mode at roughly 15% reduces unwanted wall effects. The main beam remains nearly unchanged, and cross-polarization stays low. The hybrid mode formed under these conditions contains about 85% TE_{11} and 15% TM_{11} [6, 18, 19].

In this context, the purpose of the mode converter is to convert 15% of the incident TE_{11} mode power at the input to TM_{11} mode at the output, thereby achieving an 85% TE_{11} and 15% TM_{11} balance (namely, the HE_{11} mode) at the corrugated horn input [6, 18, 19].

As such, TE_{11} is above cutoff at the input while both modes are above cutoff at the output. These restrictions are taken into account when determining the input and output radii of the mode converter. The critical parameters of the mode converter are input radius $a_{i,MC}$, output radius $a_{o,MC}$, number of slots in the mode converter N_{MC}, slot depths $d_{j,MC}$, and converter profile.

A variable-depth converter is used in the mode converter, which employs a hyperbolic profile [19]. The input and output radii of the mode converter are determined by considering both the preservation of mode conversion performance and limiting the entire size of the structure. Similar to the slot depth calculation of the corrugated horn antenna, calculations are also performed for both the Tx and Rx in the mode converter, and the average is then calculated. The input radius is 8.46 mm, and the output radius is 23 mm. The length of the converter L is 38.2 mm. Considering fabrication, the corrugation width is selected as 0.8 mm, whereas the slot width is set to 1.2 mm. The equations used in the design are provided below [19], and the mode converter is shown in Figure 2.2.

In Equation (2.1), the $a_{j,MC}(z)$ is employed to compute a location along the mode converter where the radius is . After numerous trials with different profile shapes in the mode converter, it is concluded that the hyperbolic profile is the most suitable profile for this design. In this formula, j represents the current slot. The variable z is obtained by multiplying each slot by the pitch. In this design, the pitch is 2 mm, and L represents the length. In Equation (2.2), $d_{j,MC}$ is the expression employed to calculate the slot depth in the variable-depth mode converter. Since the slot depth is required to be within the range of 0.4 to 0.5, the percentage factor σ_{MC} for the first slot depth is selected as 0.43. N_{MC} is 17, and K is denoted as the correction factor. The wavelength corresponding to the center frequency is represented by λ_c. The correction factor is defined in Equation (2.3), where k_c defines the wavenumber corresponding to the center frequency [19].

$$a_{j,MC}(z) = \sqrt{a_{i,\mathrm{MC}}^2 + \left(\frac{z}{L}\right)^2 \left(a_{o,\mathrm{MC}}^2 - a_{i,\mathrm{MC}}^2\right)} \tag{2.1}$$

$$d_{j,MC} = \left(\sigma_{\mathrm{MC}} - \frac{j-1}{N_{\mathrm{MC}}}\Big(\sigma_{\mathrm{MC}} - 0.25\,K\Big)\right)\lambda_c \tag{2.2}$$

$$K = \exp\left[\frac{1}{2.114\left(k_c\,a_{j,MC}(z)\right)^{1.134}}\right] \tag{2.3}$$

In this design, both broadband and dual-band corrugated horn antenna design approaches are investigated [19]. The most important performance criterion for the corrugated horn design presented herein is the Cross-polarization Discrimination (XPD) specification of better than 30 dB. The main parameters determining both the radiation pattern symmetry and the cross-polarization performance are the corrugation depths, their variation along the antenna, and the antenna profile [19]. The antenna section is electrically long, which facilitates the design to some degree. Cross-sectional view of the final corrugated horn and mode converter is presented in Figure 2.2.

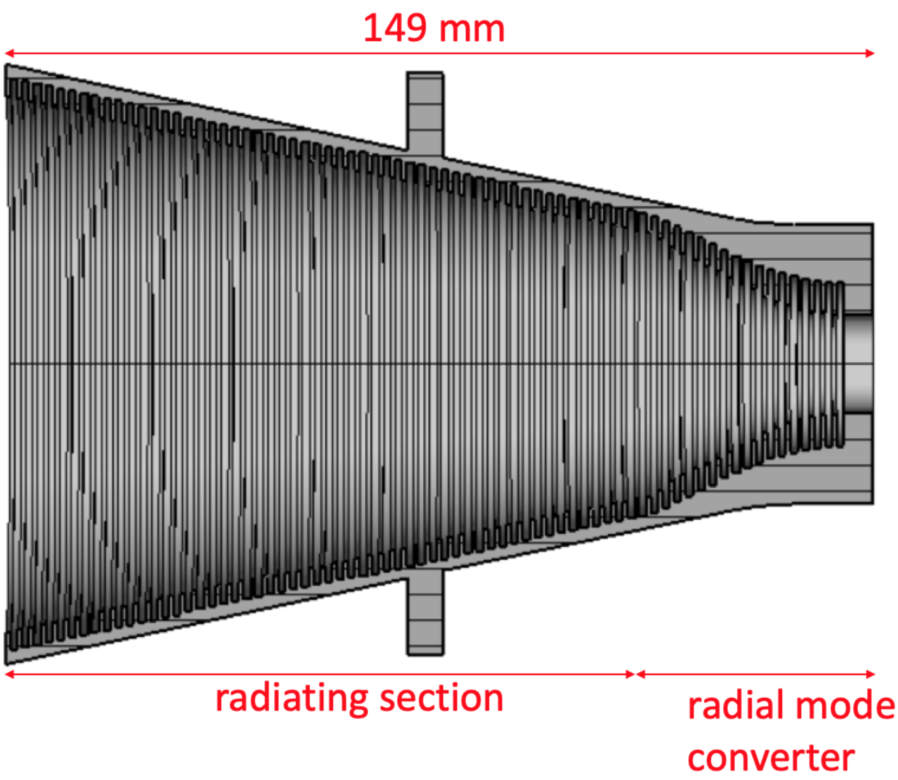

Figure 2.2: *Corrugated Horn Antenna and Radial Mode Converter.*

For the corrugation depths in the design, alternative methods presented in the literature are examined [19, 20, 21]. Consequently, the average of the two different corrugation depths determined as if designing separate corrugated horn antennas for the Rx and Tx bands is taken, and slight optimization is performed based on this. During this design, several parameters are employed, including the lowest operating frequency f_{min}, the highest operating frequency f_{max}, the center frequency, the output frequency, the input radius $a_{i,hr}$, the output radius $a_{o,hr}$, the depths of the slots $d_{j,hr}$, the corrugated horn antenna length L, the total number of corrugations N_{hr}, and the profile. The corrugated horn antenna design is performed based on these parameters, utilizing the formulas from [19], which are provided below.

In order to calculate the center frequency, both the Tx and Rx bands are considered in this design. For f_{min}, 17.7 GHz is utilized for the Tx band and 27.5 GHz for the Rx band. For f_{max}, 20.2 GHz is employed in the Tx band and 30 GHz in the Rx band. This can be seen in Equation (2.4). f_o is the output frequency, and the corresponding expression is shown in Equation (2.5). So as to compute both the wavelength of the center frequency and the wavelength of the output frequency, Equation (2.6) and Equation (2.7) are used. Since a linear surface profile is selected to design the corrugated horn antenna, Equation (2.8) is obtained by calculating the corrugated horn antenna's input and output radii, length, and z parameters. In order to determine the slot depth of this antenna, Equation (2.9) is employed, which includes the surface profile, wavelength, and wavenumber [19].

$$f_c = \sqrt{f_{min}\, f_{max}} \tag{2.4}$$

$$f_o = 1.025\, f_c \tag{2.5}$$

$$\lambda_c = \left(\frac{c}{f_c}\right),\ k_c = \frac{2\pi}{\lambda_c} \tag{2.6}$$

$$\lambda_o = \left(\frac{c}{f_o}\right),\ k_o = \frac{2\pi}{\lambda_o} \tag{2.7}$$

$$a_{j,hr}(z) = a_{i,hr} + \left(a_{o,hr} - a_{i,hr}\right)\frac{z}{L} \tag{2.8}$$

$$d_{j,hr} = \frac{\lambda}{4}\,\exp\left[\frac{1}{2.114\left(k\, a_{j,hr}\right)^{1.134}}\right] \tag{2.9}$$

Since there are two different frequency bands in this design, many of the formulas employed are calculated separately for both Rx and Tx bands. In this thesis, the formulas are not expressed separately for Rx and Tx; they are presented in a generalized form as an example of the formulas employed. As a result, even though the same parameter names are used for both the corrugated horn antenna and the mode converter, the calculations are different.

The total number of corrugations is 72. The corrugation depth decreases from half a wavelength at the input of the mode converter to a quarter of a wavelength along the structure [19]. The corrugated horn antenna profile is linear, and the flare angle of the linear profile is kept within 10-15 degrees to reduce mode conversion within the antenna [6, 19].

Figure 2.3 presents both return loss and cross-polarization discrimination of the horn with the mode converter. The return loss is better than 25 dB, and the cross-polarization discrimination is over 39 dB across the entire frequency range.

Co-polar and cross-polar radiation patterns are analyzed at 0.5 GHz intervals in both frequency bands. Figures 2.4 and 2.8 present Tx co-polarized gain patterns for both RHCP and LHCP polarizations, respectively, in $\phi = 0°, 45°, 90°$ planes. Figures 2.6 and 2.10 present Rx co-polarized patterns in the same planes. Tx and Rx co-pol gain is approximately 27.5 and 29.5 dBi, respectively. The back lobe level across all co-polar radiation patterns is nearly 50 dBc across both bands, and the sidelobe level is better than the target value of 30 dBc.

Figures 2.5 and 2.9 present Tx cross-polarized gain patterns for both RHCP and LHCP polarizations, respectively, in $\phi = 0°, 45°, 90°$ planes. Figures 2.7 and 2.11 display the same curves for the Rx RHCP and LHCP polarizations, respectively. These four figures clearly show the excellent cross-polarization discrimination of the corrugated horn in all ϕ planes.

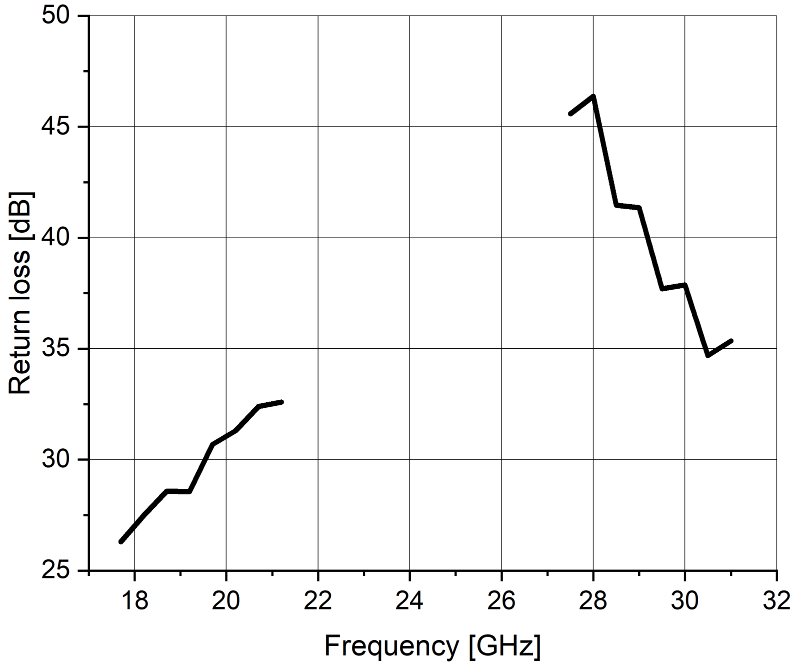

(a)

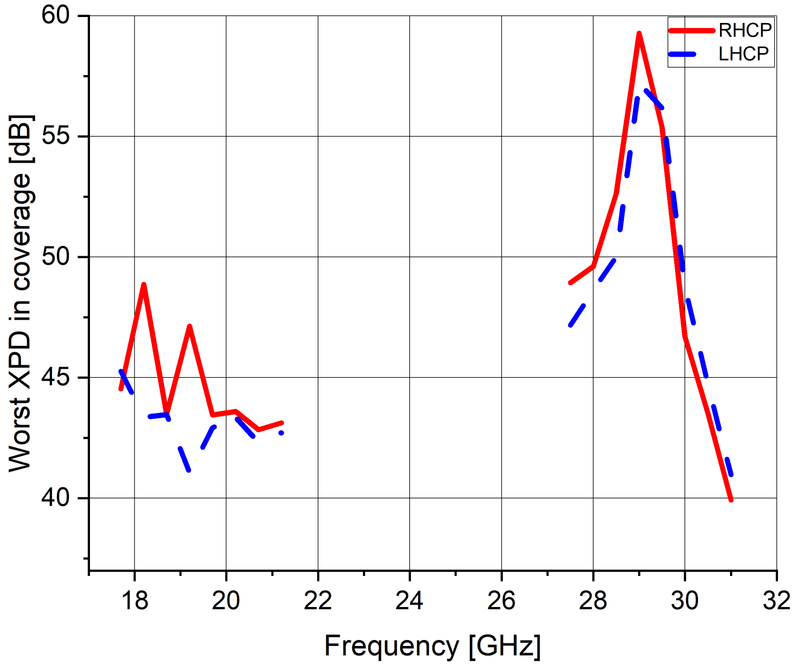

(b)

Figure 2.3: *(a) Return Loss and (b) XPD of the Corrugated Horn and Mode Converter.*

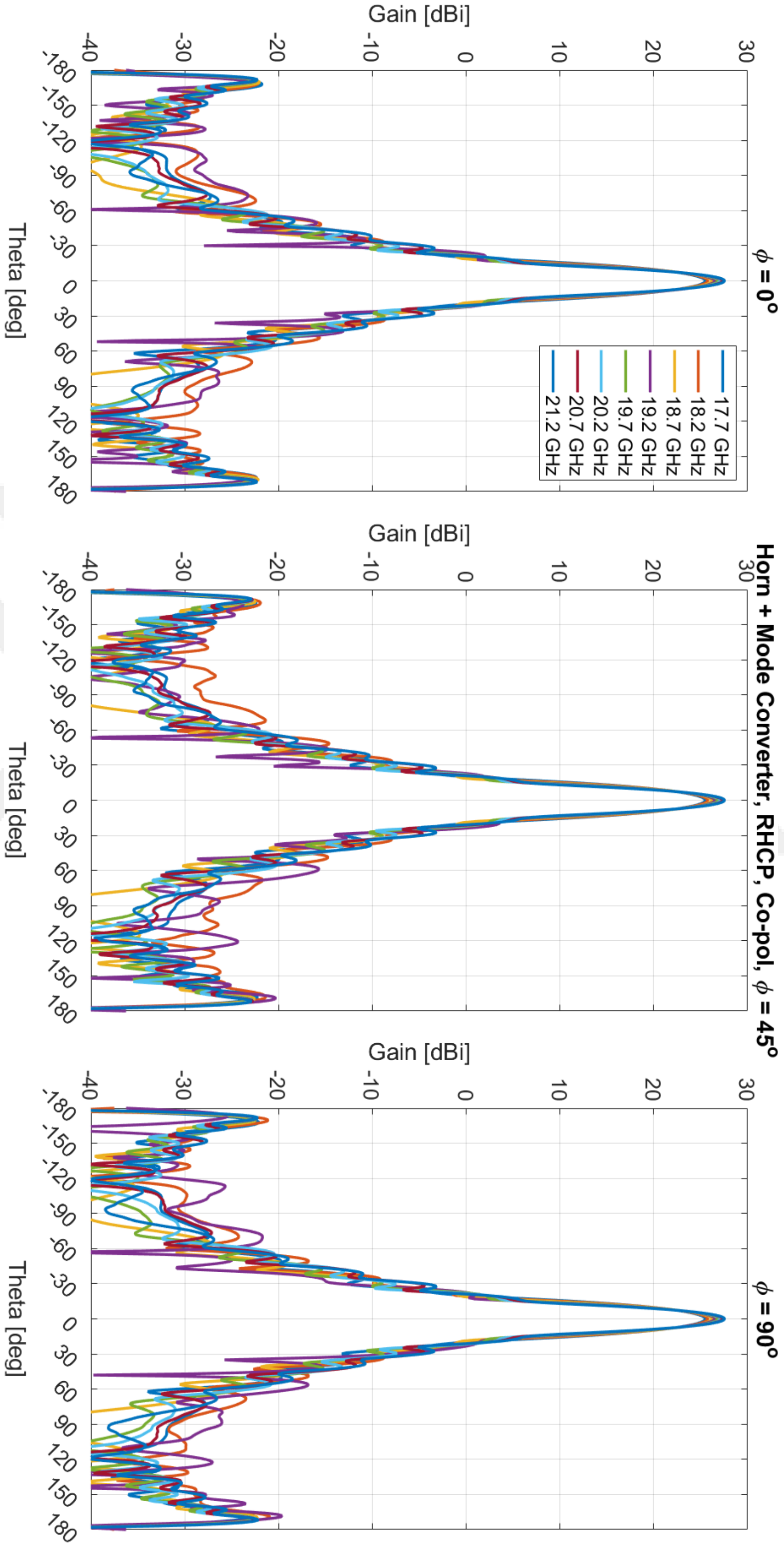

Figure 2.4: *Tx Co-polarized (RHCP) Radiation Patterns.*

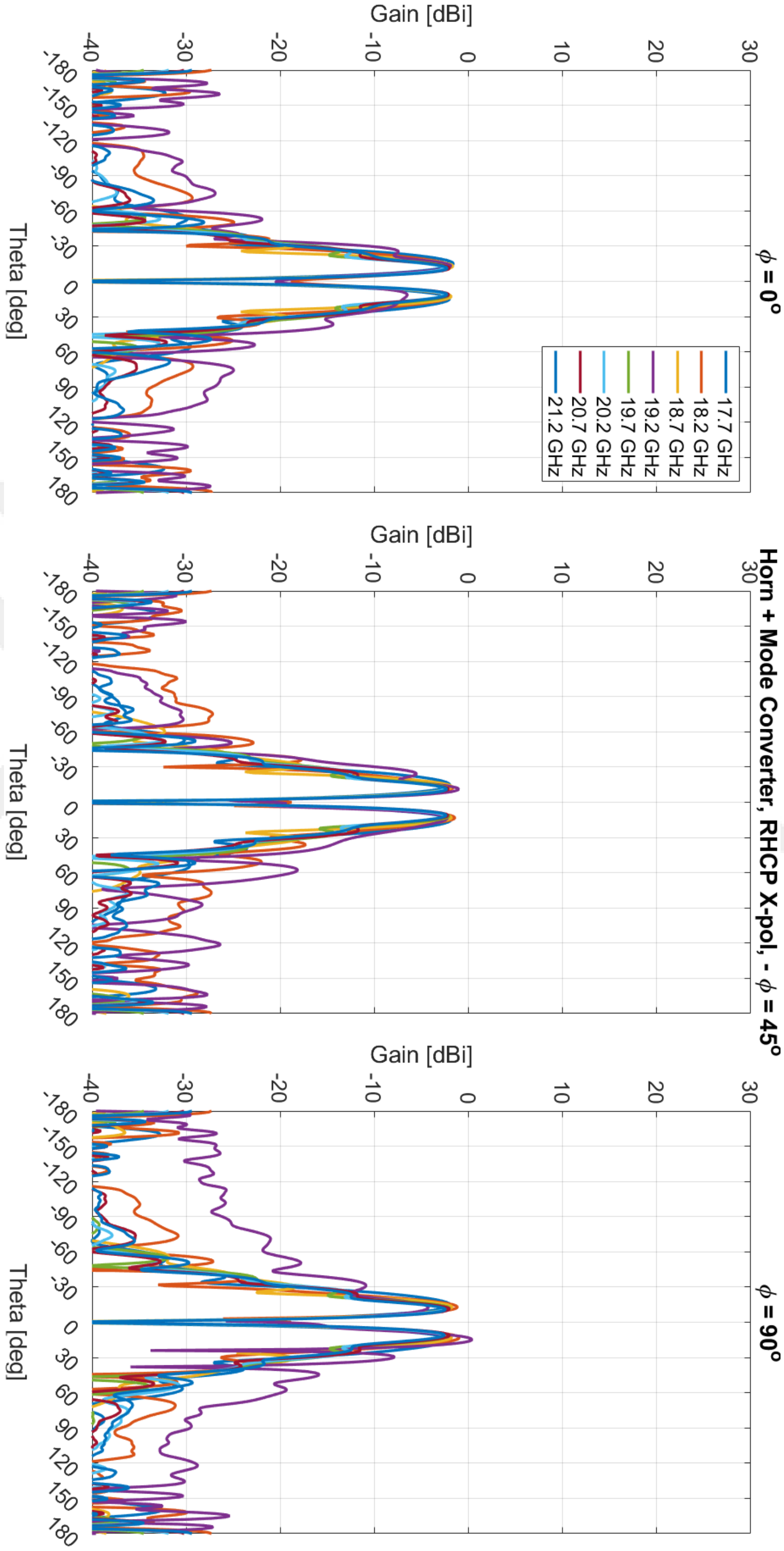

Figure 2.5: *Tx Cross-polarized (RHCP) Radiation Patterns.*

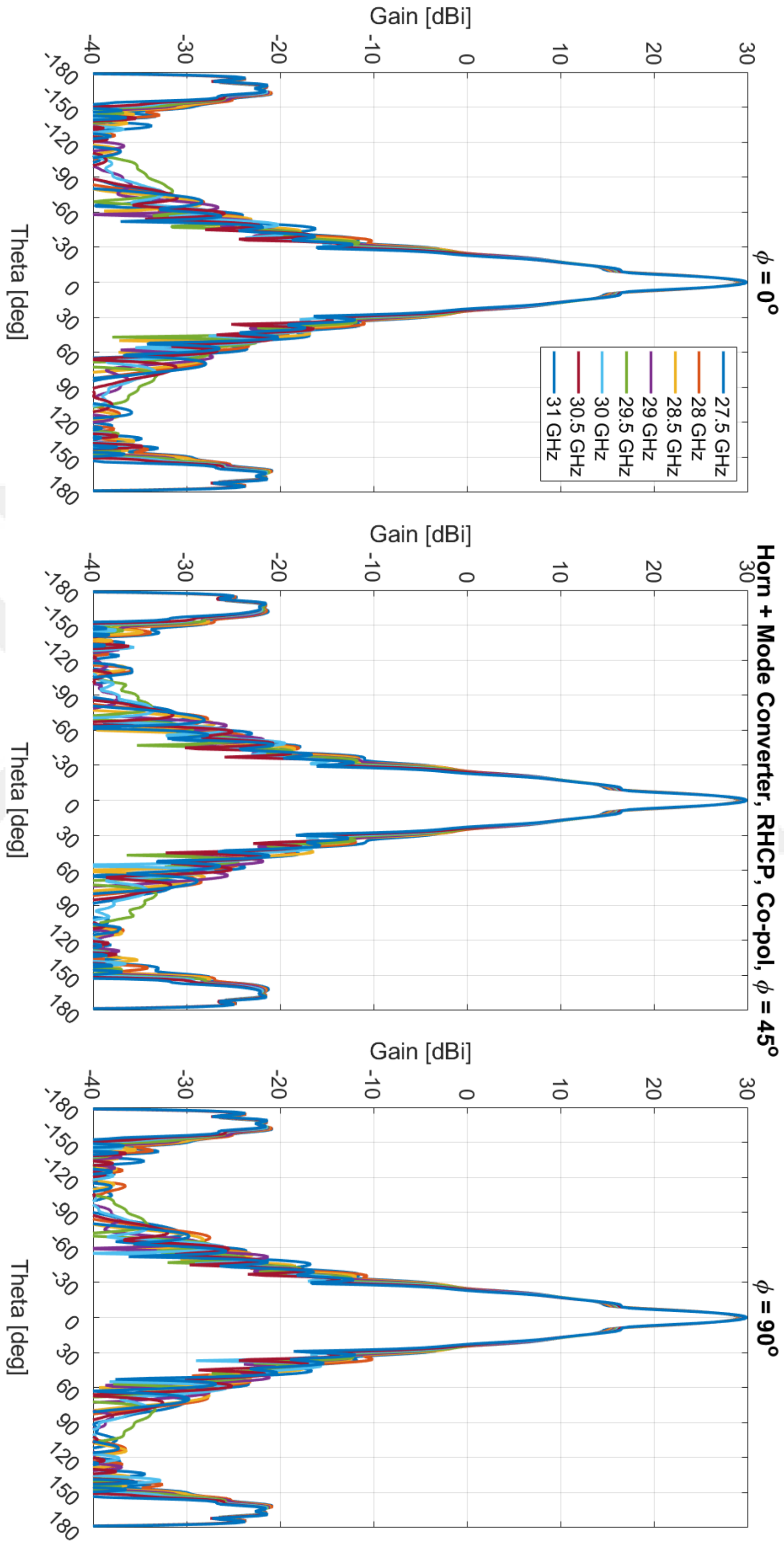

Figure 2.6: *Rx Co-polarized (RHCP) Radiation Patterns.*

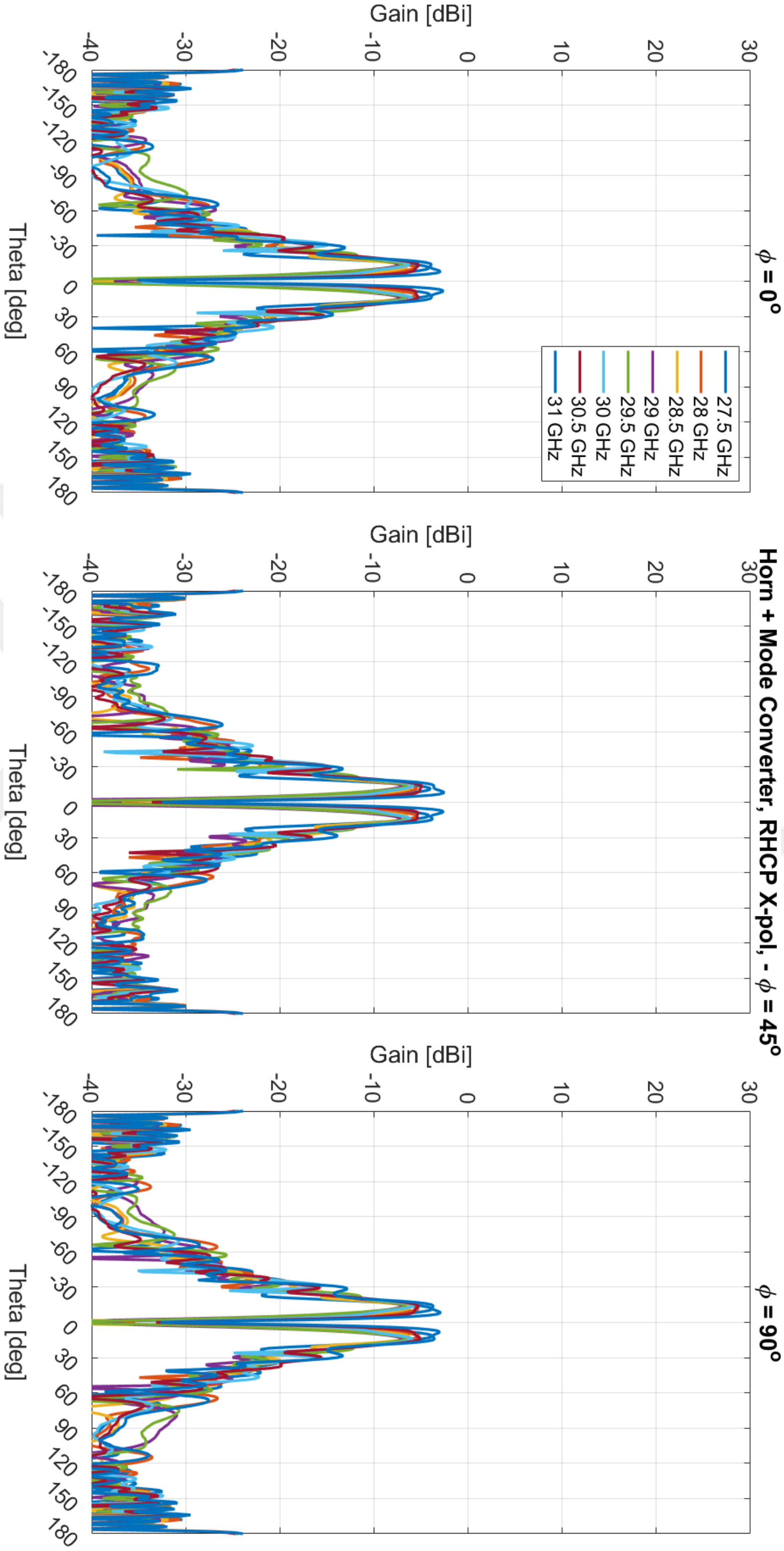

Figure 2.7: *Rx Cross-polarized (RHCP) Radiation Patterns.*

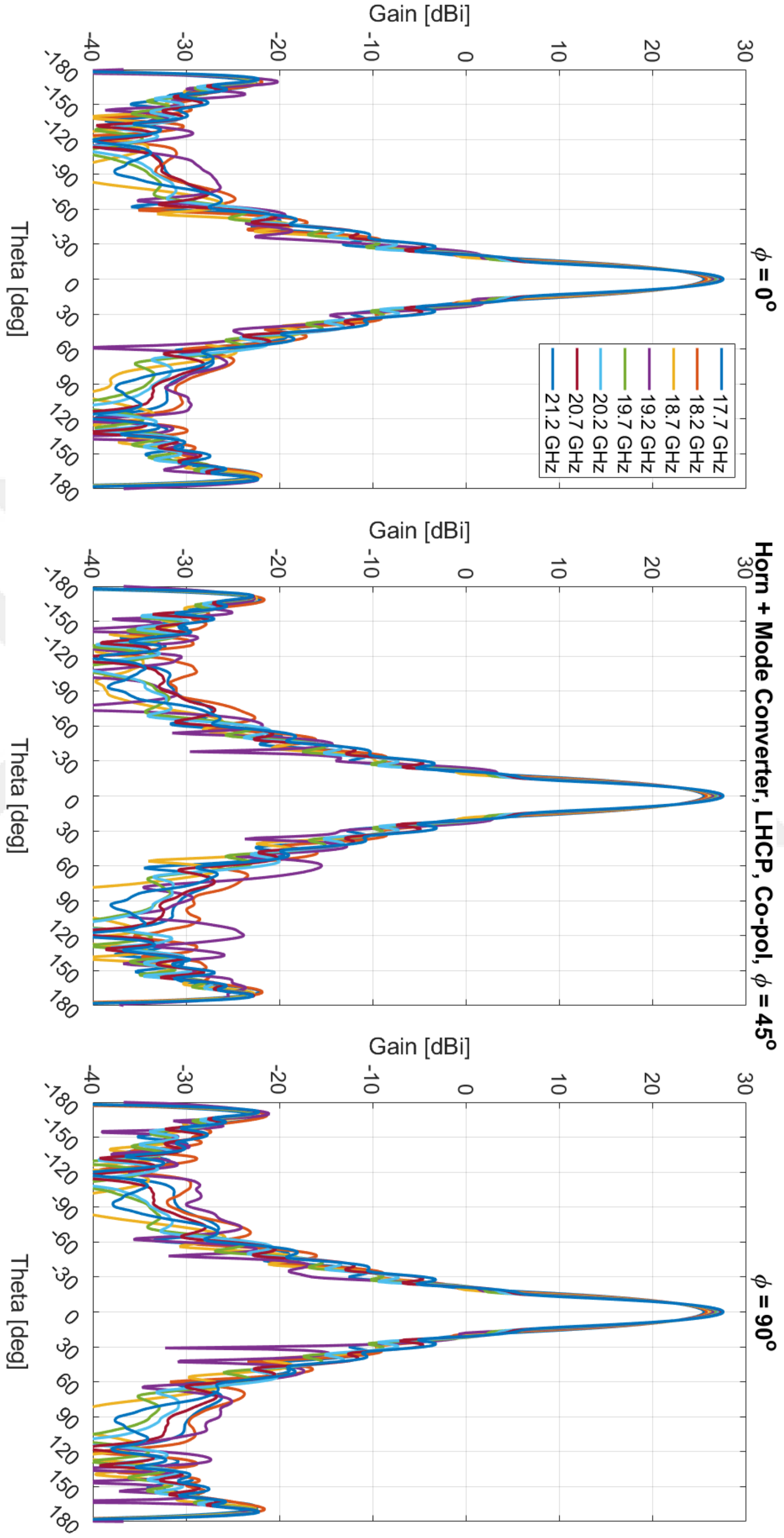

Figure 2.8: *Tx Co-polarized (LHCP) Radiation Patterns.*

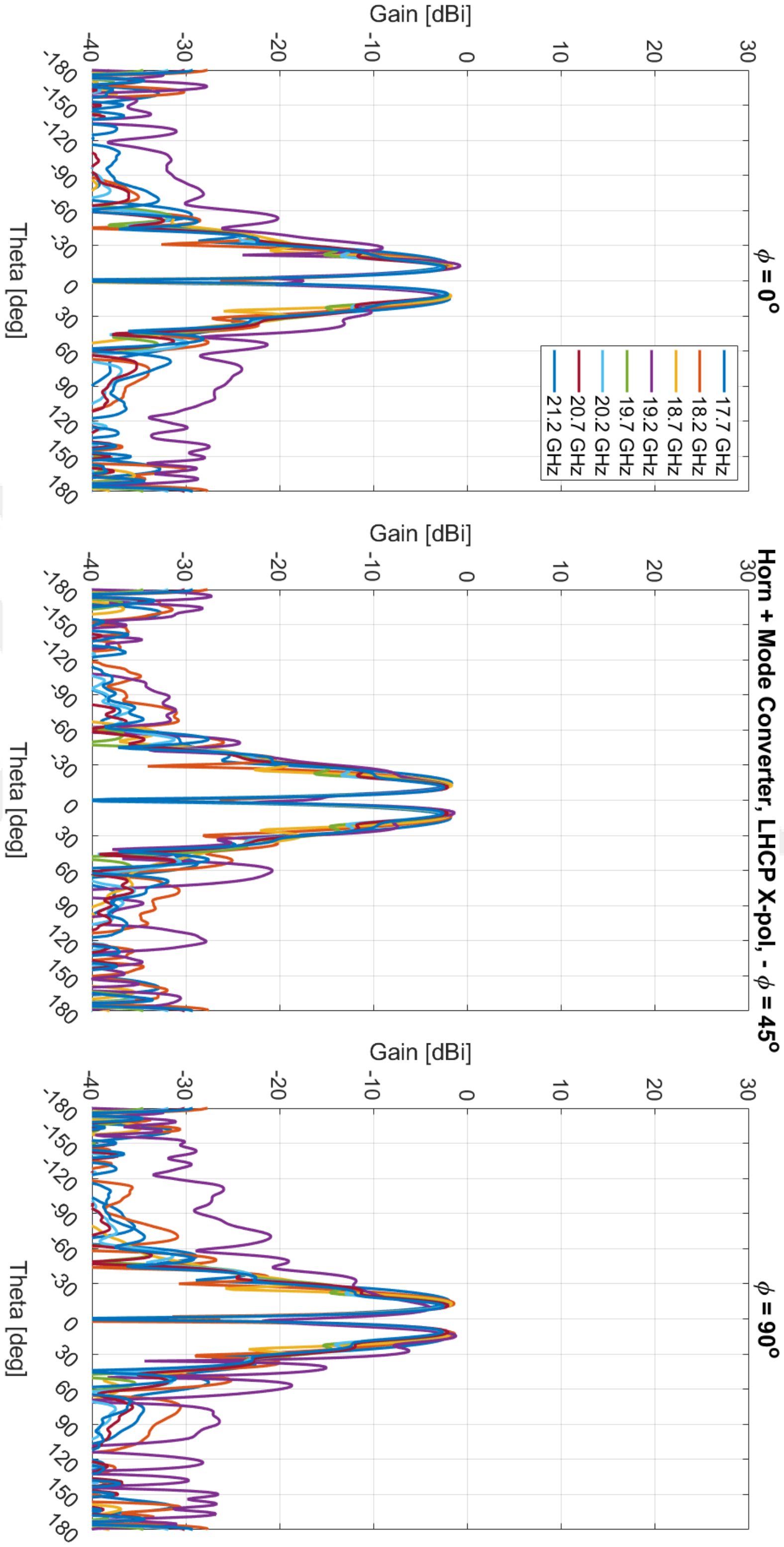

Figure 2.9: *Tx Cross-polarized (LHCP) Radiation Patterns.*

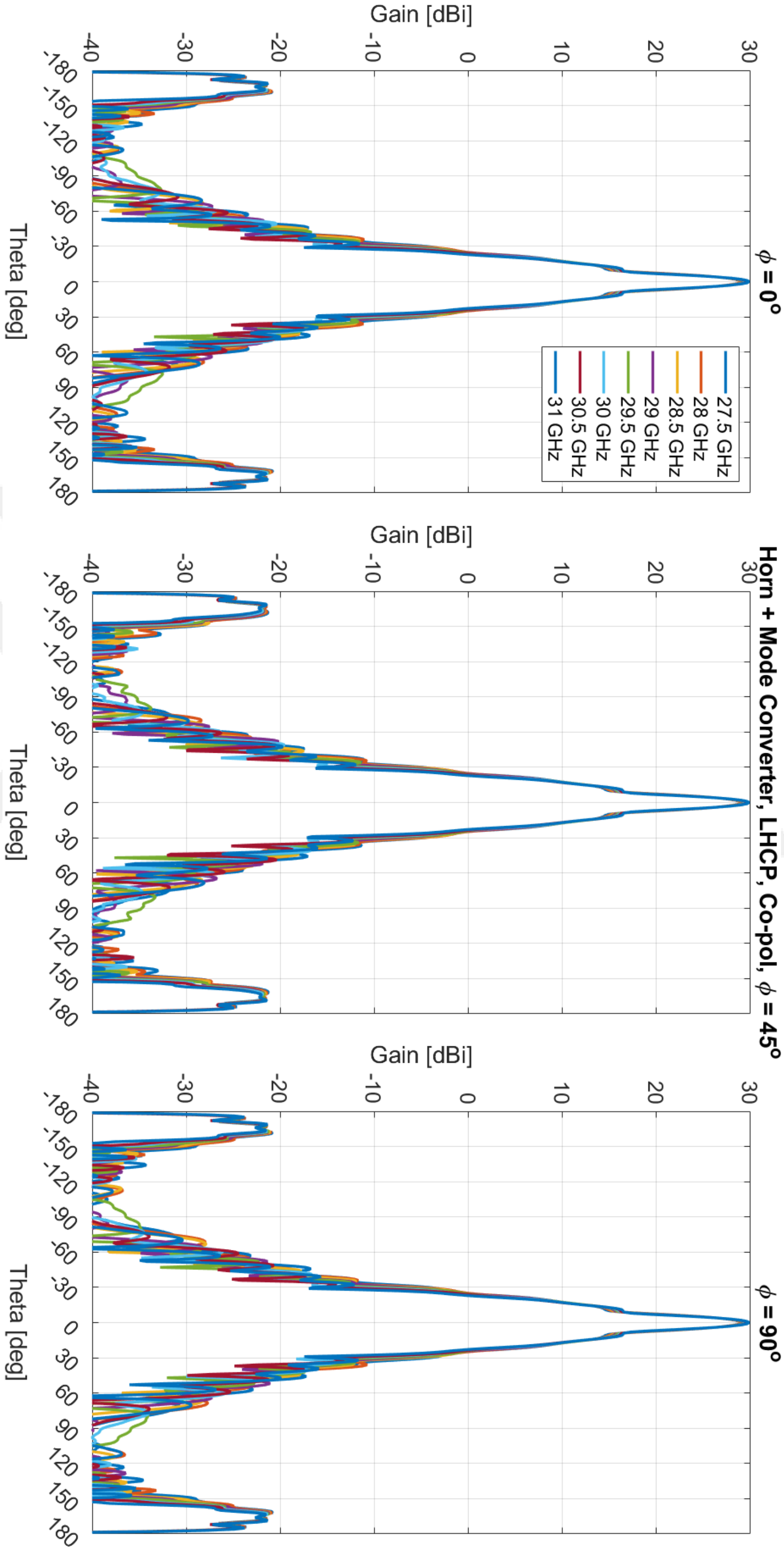

Figure 2.10: *Rx Co-polarized (LHCP) Radiation Patterns.*

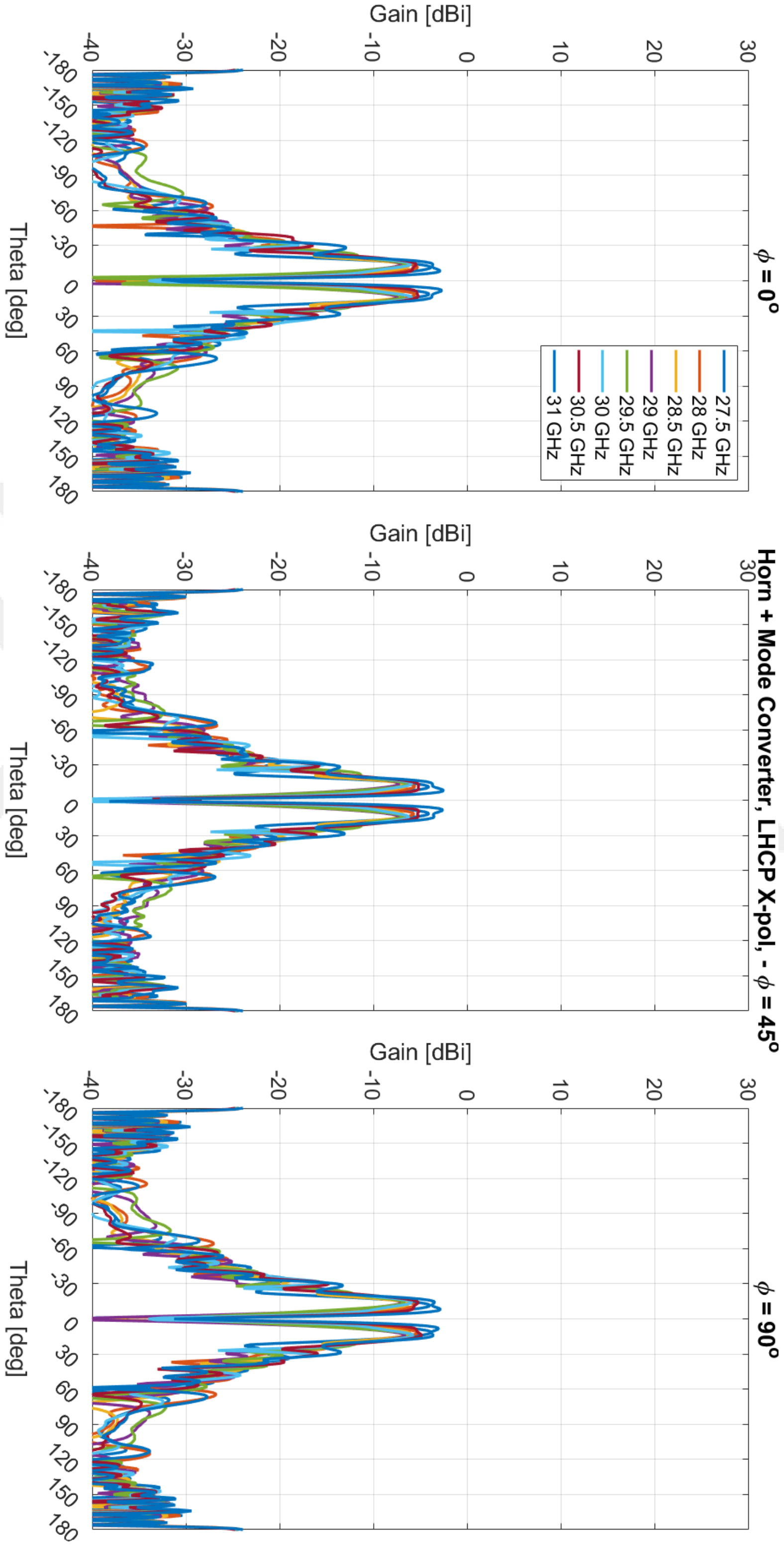

Figure 2.11: *Rx Cross-polarized (LHCP) Radiation Patterns.*

2.2 Feed Network

2.2.1 *Circular-to-Square Waveguide Transition*

A circular-to-square waveguide transition is used between the radial mode converter and the six-port ortho-mode junction. This waveguide transition is implemented employing a lofted geometry between a circular waveguide and a square waveguide. The circular waveguide is matched to the input of the radial mode converter, whereas the square waveguide interface of this design is compatible with the six-port OMJ. This approach facilitates a gradual transition, which enhances impedance matching and reduces excitation of higher-order waveguide modes. The vacuum model of the structure is shown in Figure 2.12.

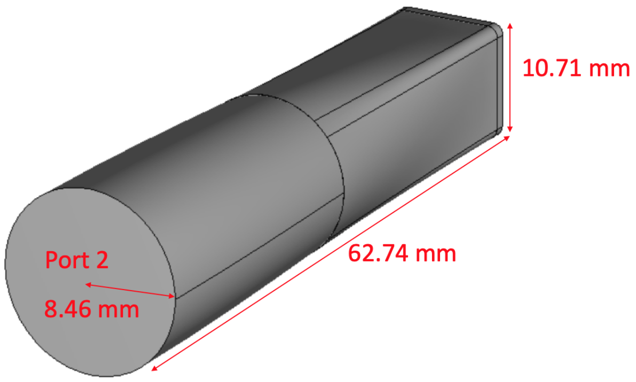

Figure 2.12: *Vacuum Model of the Circular-to-square Waveguide Transition.*

As shown in Figure 2.13, the transition presents a return loss exceeding 50 dB. The primary goal in the design of this circular-to-square waveguide transition is to minimize return loss while minimizing mode conversion within the circular-to-square waveguide transition. This approach aims to reduce losses that may degrade the cross-polarization discrimination. The square section of this component, namely Port 1, is connected to the six-port OMJ, while Port 2 is connected to the radial mode converter. Mode #7 at Port 2 corresponds to TM_{11}, while at Port 2, mode #9 represents TE_{31} [22]. These two modes are presented because they can be easily excited in the transition. Insertion loss exceeding 30 dB for these (and all other higher-order modes) ensures minimal mode conversion losses in the circular-to-square waveguide transition.

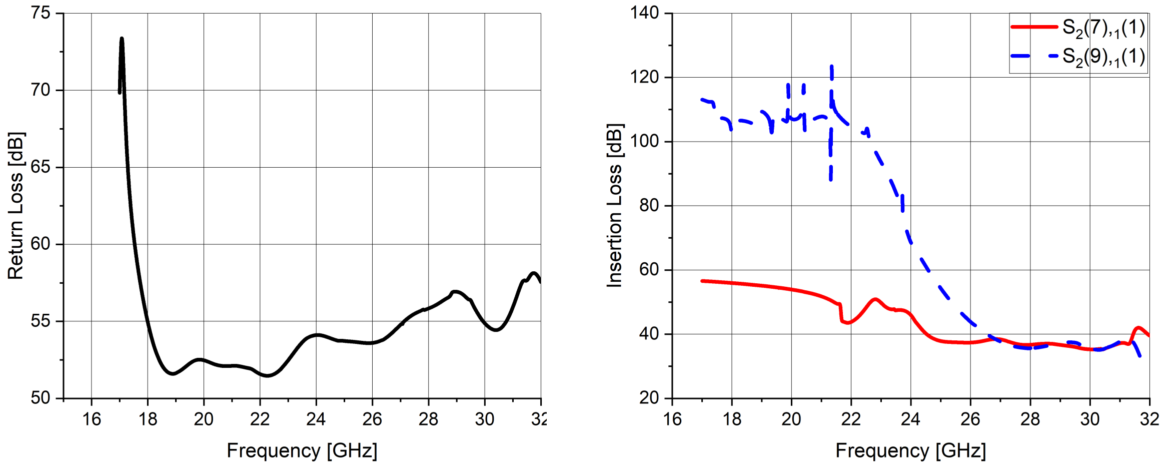

(a) (b)

Figure 2.13: *(a) Return Loss of TE_{11} Mode of the Circular-to-square Waveguide Transition (b) Insertion Loss of TM_{11} (Red) and TE_{31} (Blue) Modes.*

2.2.2 Six-port Ortho-mode Junction

An OMJ is a passive component employed to combine or separate two signals transmitted in orthogonal polarizations [9]. The signal in the Tx and Rx bands is diplexed within this section [7]. It also plays an efficient role in achieving dual circular polarization [11]. This design uses rectangular waveguides with different dimensions. To ensure proper separation of the signals received from the antenna, the cutoff frequency should be less than 17.7 GHz for the low-frequency band and less than 27.5 GHz for the high-frequency band. The fundamental mode must be supported at the lowest frequency, while higher-order modes must be suppressed at the highest frequency [7]. Parameter calculations are carried out based on these requirements.

Figure 2.14 presents a detailed view of the component. Port 1 is the square section connected to the circular-to-square waveguide transition. The arm ports are labeled Port 2, Port 3, Port 4, and Port 5. Ports 2 and 4, and likewise Ports 3 and 5, are positioned opposite each other. Port 6 is where the connection to the high-band septum is made. The Tx signals (two polarizations) arriving from the four arms are combined at the six-port OMJ. The arms of the six-port OMJ comprise three stepped waveguide sections. The iris, narrowest of the three sections, plays an essential role in coupling the Tx signal from the arms to the six-port OMJ. Blends have also been applied to the rectangular waveguide, with a radius of 0.6 mm. The iris and its adjacent structures are designed such that their combined length is at least 6.25 mm to ease fabrication. Waveguide width and height of the arms are 9.4 mm and 3 mm, respectively. The Rx band signal propagates from the circular-to-square transition into the six-port OMJ and straight through Port 6 to the Rx septum polarizer.

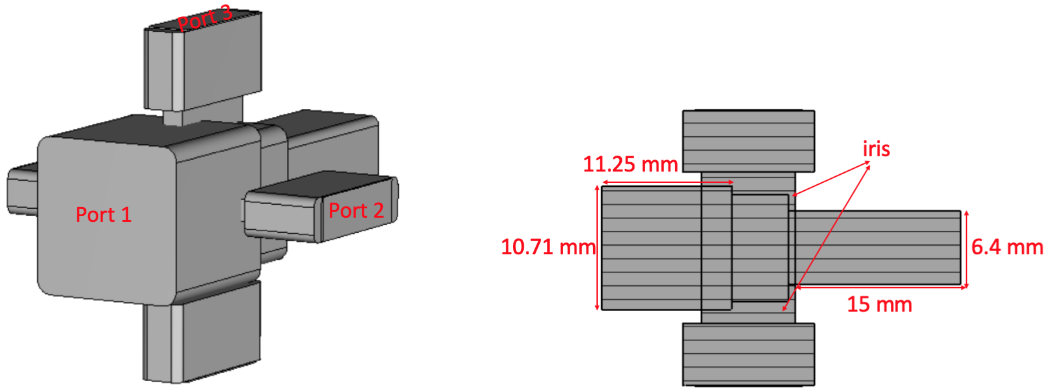

(a) (b)

Figure 2.14: *(a) Perspective and (b) Cross-sectional View of Vacuum Model of the Six-port OMJ.*

As shown in Figure 2.15, the return loss of the six-port OMJ is greater than 20 dB in both Tx and Rx bands. S_{31} of this structure is 3 dB, and the S_{61} value is 0 dB, as illustrated in Figure 2.15, because while the signals operating in the low-frequency band coming from the arms are combined in the six-port OMJ, the signals in the high-frequency band propagate straight to the septum polarizer.

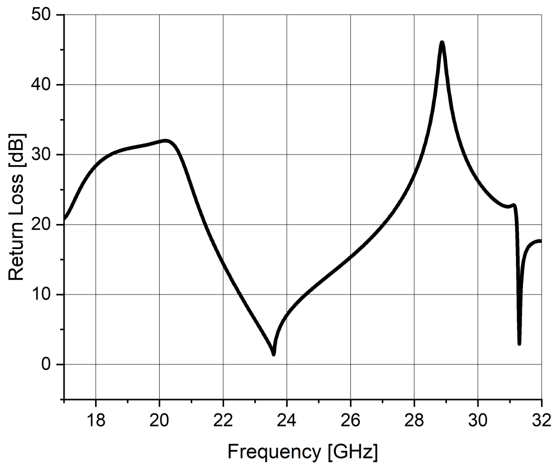

(a)

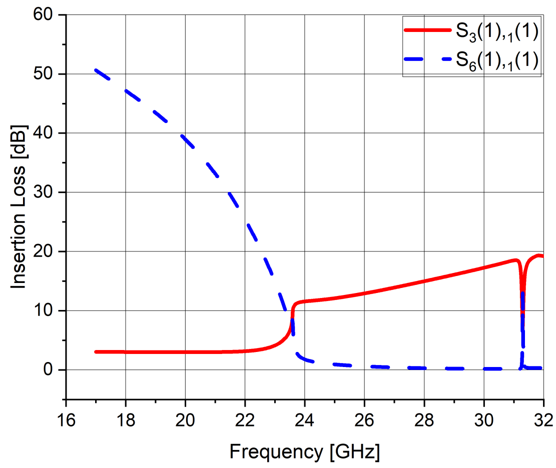

(b)

Figure 2.15: *(a) Return Loss of the Dominant Mode at Port 1 of the Six-port OMJ (b) Insertion Loss from Port 1 to Port 3 (One of the Low-band Arms, Red) and Port 6 (High-band Interface, Dashed Blue).*

2.2.3 Waveguide Low-pass Filters

In this design, corrugated waveguide low-pass filters are employed on the four Tx arms of the feed network to prevent high-frequency signals from leaking into the low-frequency section of the feed [23]. The filters are designed considering the maximum passband frequency, return loss, insertion loss, out-of-band rejection level, and the stop-band lower limit [24].

In this structure, a total of eight waveguide low-pass filters of two distinct geometries are employed to prevent high-frequency signals that can leak into the low-frequency arms of the six-port ortho-mode junction. Four of the eight filters are placed immediately after the arms of the six-port ortho-mode junction to suppress resonances that may occur within the six-port OMJ. These filters, consisting of 9 sections, are slightly smaller than the remaining four, with a length of 21.36 mm. This approach reduces the occupied space while effectively suppressing resonances. The vacuum model of the filter is illustrated in Figure 2.16. Figure 2.17 presents the scattering parameters of these filters. The cutoff frequency is 23.5 GHz, and the out-of-band rejection level is better than 20 dB in the 27.5-31 GHz range, and return loss is above 30 dB.

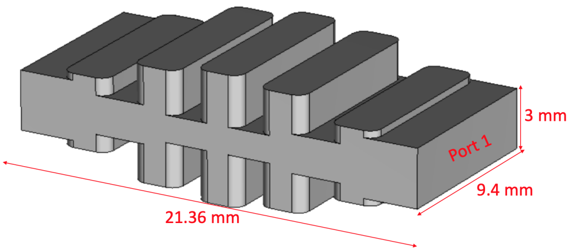

(a)

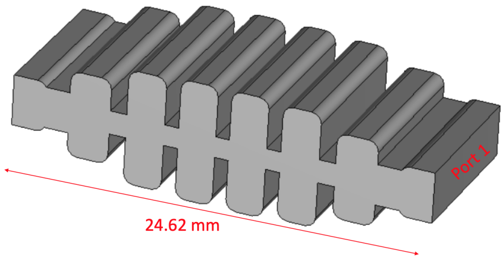

(b)

Figure 2.16: *Vacuum Models of the Corrugated Waveguide Low-pass Filter with (a) 9 Sections, (b) 13 Sections.*

The remaining four filters facilitate most of the out-of-band isolation of the overall feed network. They comprise 13 sections and are 24.62 mm long. The vacuum model of this filter design is also depicted in Figure 2.16. As illustrated in Figure 2.17, return loss is in excess of 30 dB. Similar to the other waveguide low-pass filter, the cutoff frequency is 23.5 GHz, and the out-of-band rejection level exceeds 50 dB in the 27.5-31 GHz range.

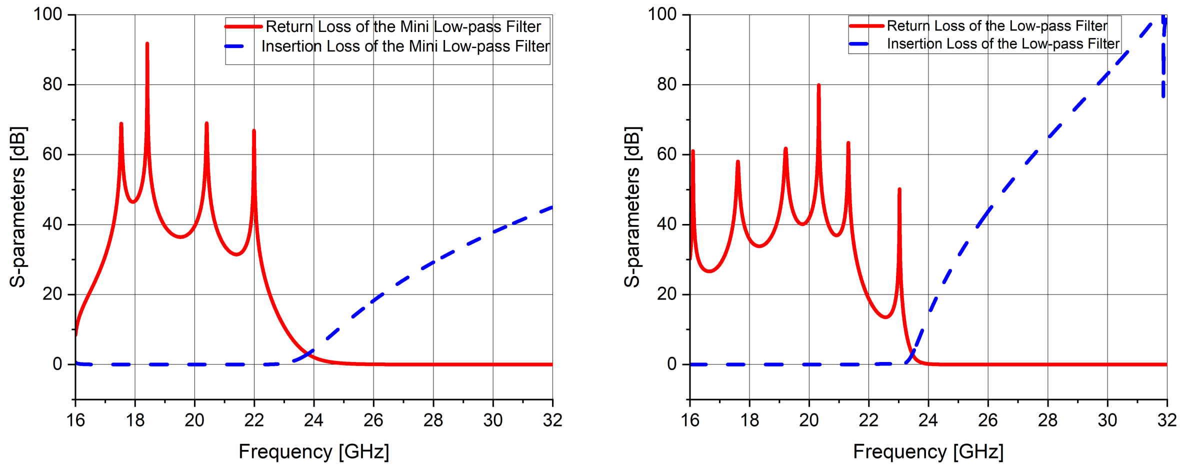

(a) (b)

Figure 2.17: *Return Loss and Insertion Loss of the Waveguide Low-pass Filter with (a) 9 Sections, (b) 13 Sections.*

2.2.4 Five-port Ortho-mode Junction

The five-port OMJ includes a combination of rectangular waveguides with varying dimensions, similar to the six-port OMJ. Two linear Tx polarizations from the Tx septum polarizer are split into four arms in the five-port OMJ. Thereby, this component effectively acts as a turnstile-type power divider [7]. As in the six-port OMJ, the five-port OMJ is symmetric, and identical results are obtained from the opposite ports. The interface between the structure and the low-band septum polarizer is square-shaped. Figure 2.18 demonstrates a detailed illustration. A blend with a radius of 0.6 mm is employed. The distance between the square-shaped interface and the rectangular waveguide is maintained at approximately 1 mm to avoid excessively narrow spacing. The total length of a section of the iris extending from the square-shaped interface and the adjacent rectangular waveguide is adjusted to 4.78 mm.

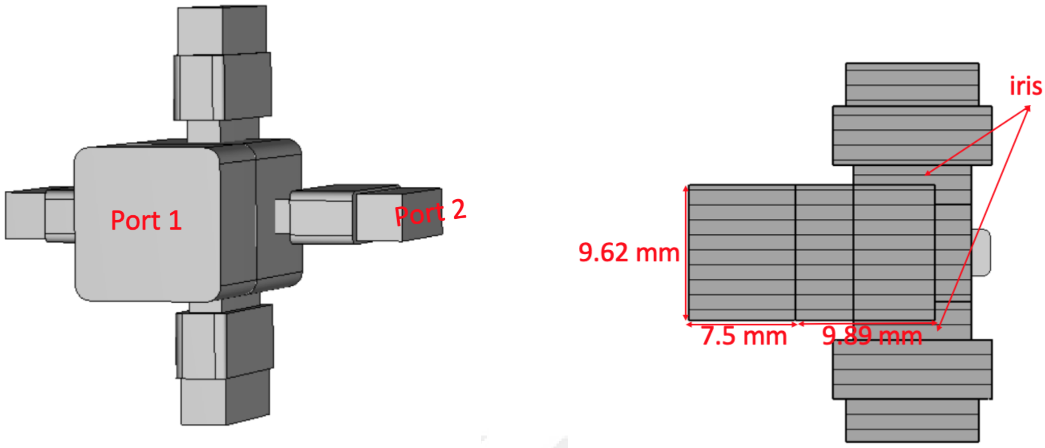

(a) (b)

Figure 2.18: *(a) Perspective and (b) Cross-sectional View of Vacuum Model of the Five-port OMJ.*

As shown in Figure 2.19, the return loss exceeds 30 dB, and the insertion loss is approximately 3 dB. These results confirm the structural symmetry and indicate that the opposite ports are identical.

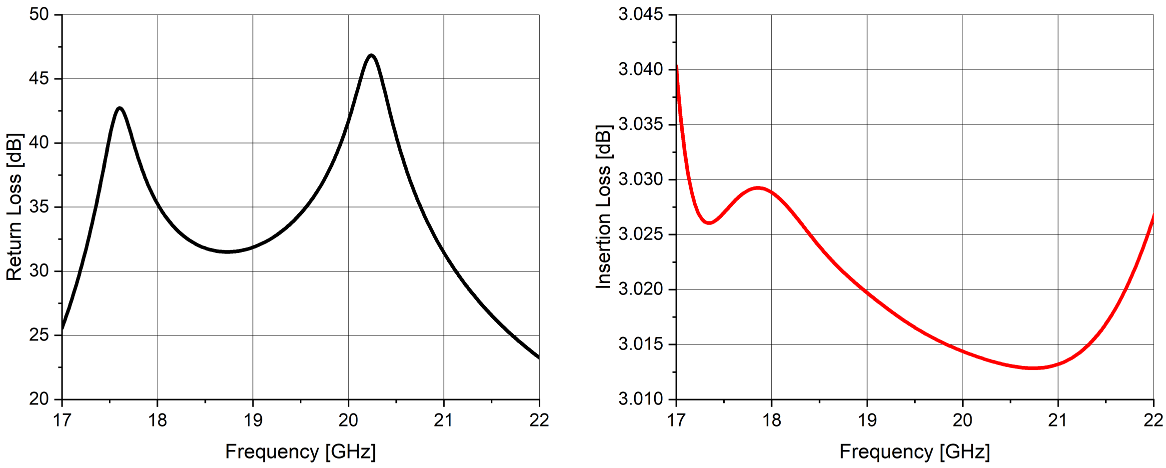

(a) (b)

Figure 2.19: *(a) Return Loss of the Dominant Mode at Port 1 of the Five-port OMJ (b) Insertion Loss of the Five-port OMJ.*

2.2.5 Septum Polarizers

Two separate septum polarizers for the Tx and Rx bands have been designed. These septum polarizers are employed to generate circular polarization. Septum polarizers contain a septum waveguide with a square-shaped front section, a multi-step conductive septum, and a section designed for the LHCP and RHCP ports [25]. Specific parameters are considered during the design of septum polarizers. These consist of septum thickness, the lengths of the steps, the gaps between the steps, and the internal dimensions of the waveguide.

The vacuum model of the high-band septum polarizer is shown in Figure 2.20. As shown in Figure 2.21, the return loss is over 30 dB. The magnitude difference between the TE_{10} and TE_{01} modes is observed to be nearly zero, as shown in Figure 2.22. Also displayed in the same figure is the phase deviation between the two output modes, which is seen to be within ±2.5° in the Rx band.

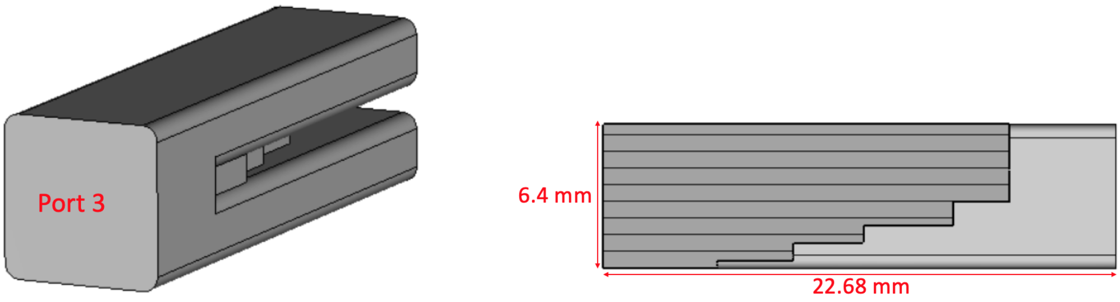

(a) (b)

Figure 2.20: *(a) Perspective, (b) Cross-sectional View of Vacuum Model of the Rx Septum Polarizer.*

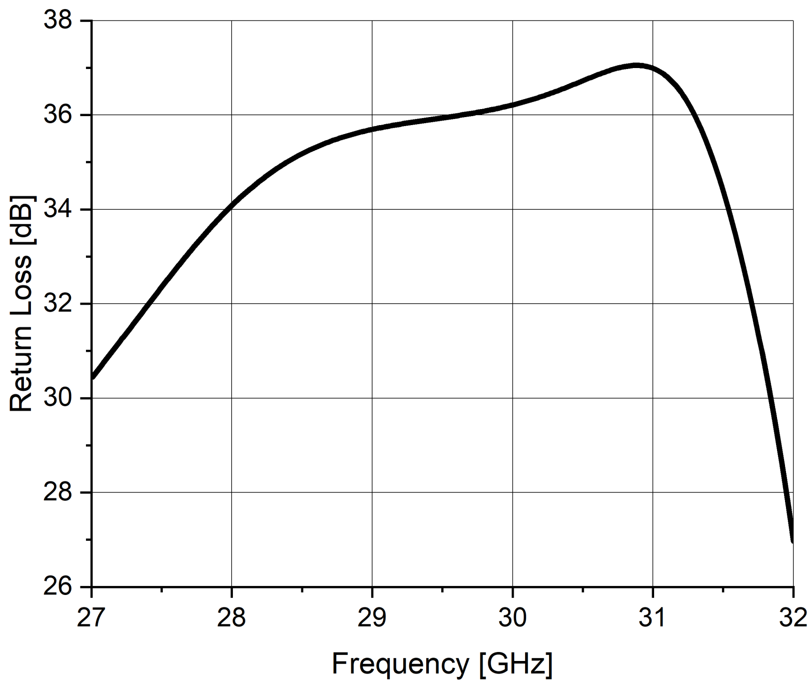

Figure 2.21: *Return Loss in dB vs. Frequency of the Rx Septum Polarizer.*

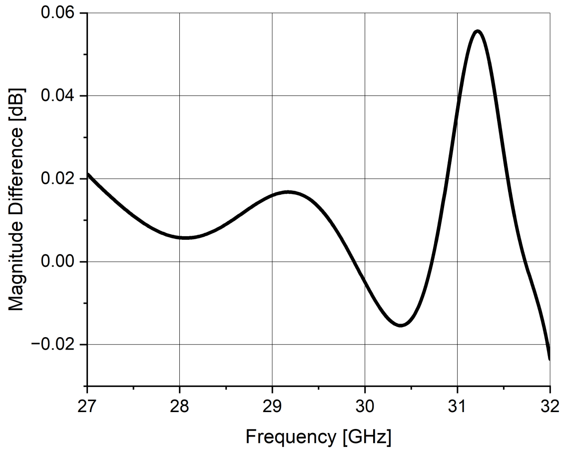

(a)

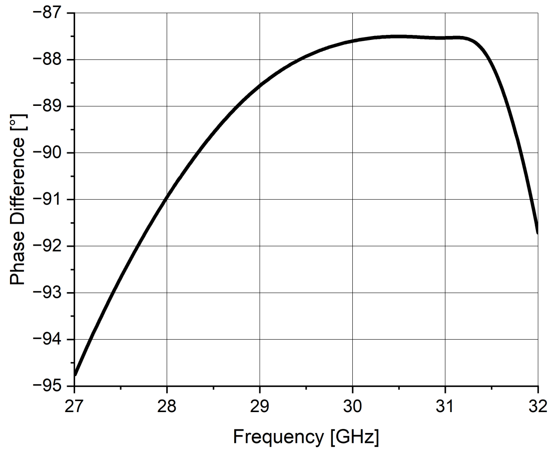

(b)

Figure 2.22: *(a) Magnitude and (b) Phase Difference Between TE_{10} and TE_{01} Modes at the Rx Septum Polarizer Output.*

The low-band septum polarizer has been designed in the same manner. Figure 2.23 presents the structure of the low-band septum polarizer. The return loss of this septum polarizer can be seen in Figure 2.24. The magnitude difference is also nearly 0 dB as a high-band septum polarizer, which is shown in Figure 2.25. In the same manner as the other, the phase deviation is reduced to about ±4° as illustrated in Figure 2.25. The square section of the low-band septum polarizer has a side length of 9.62 mm and a length of 30.12 mm. For the high-band septum polarizer, the square section measures 6.4 mm on each side and has a length of 22.68 mm.

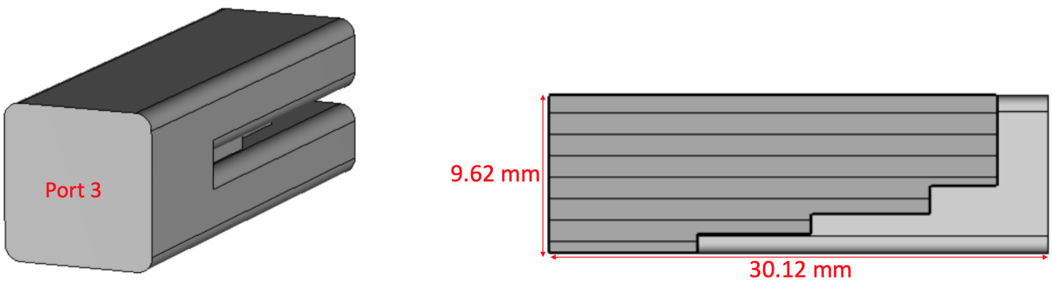

(a) (b)

Figure 2.23: *(a) Perspective, (b) Cross-Sectional View of Vacuum Model of the Tx Septum Polarizer.*

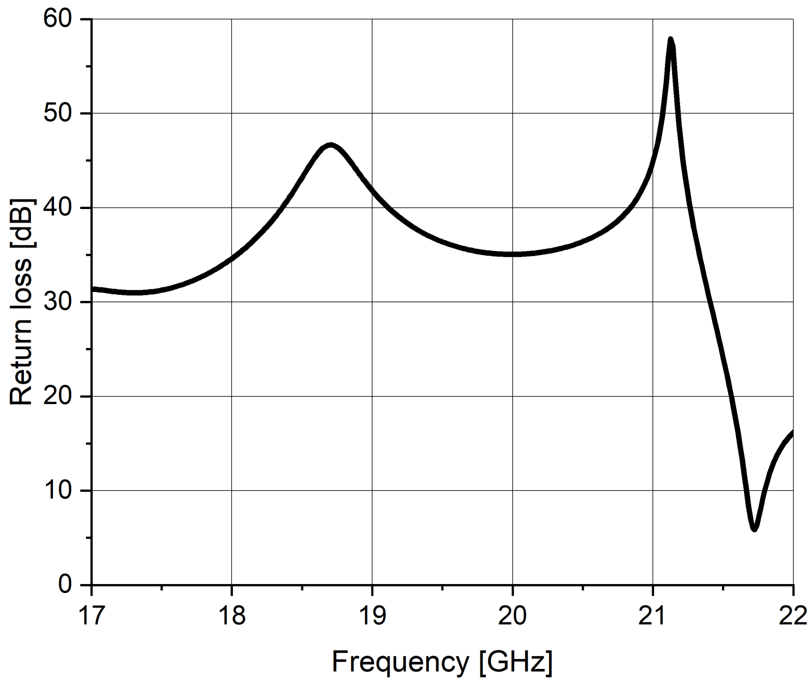

Figure 2.24: *Return Loss in dB vs. Frequency of the Tx Septum Polarizer.*

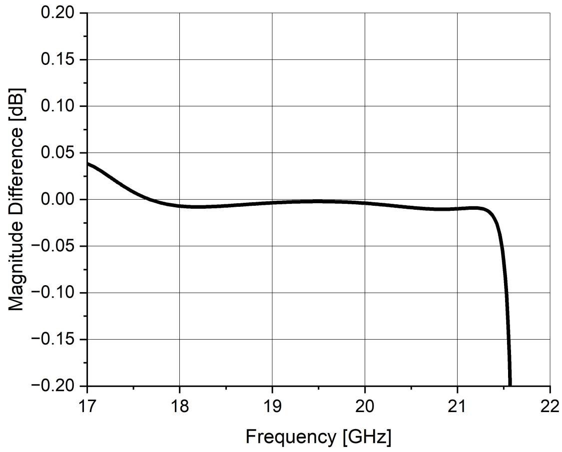

(a)

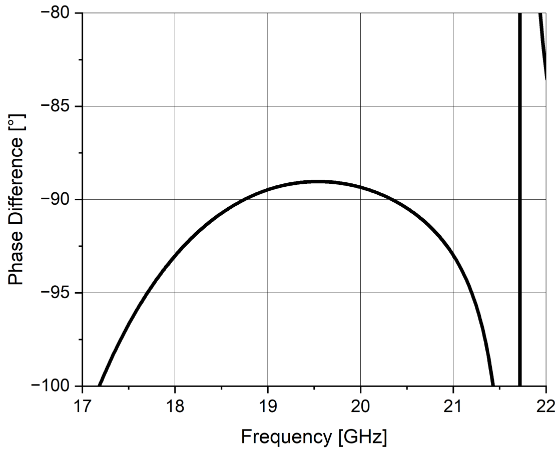

(b)

Figure 2.25: *(a) Magnitude and (b) Phase Difference Between TE_{10} and TE_{01} Modes at the Tx Septum Polarizer Output.*

2.2.6 H-plane Bends

Tx signals, split in the five-port OMJ, are guided toward the H-plane bends, filtered through the waveguide low-pass filters, subsequently combined in the six-port OMJ, transition through the circular-to-square waveguide transition, and are eventually transmitted to the antenna section. It is employed for changing the direction of wave propagation in the waveguide. The bends are designed in a stepped manner, including three discrete steps. At each step, blends with a radius of 0.6 mm are used as part of the design. Figure 2.26 describes the H-plane bend designed before the waveguide low-pass filter with fewer sections. As shown in Figure 2.26, the return loss is greater than 35 dB.

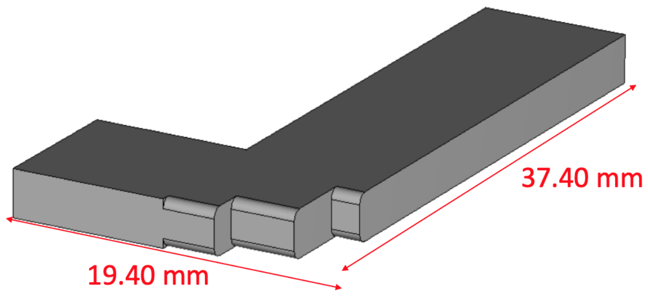

(a)

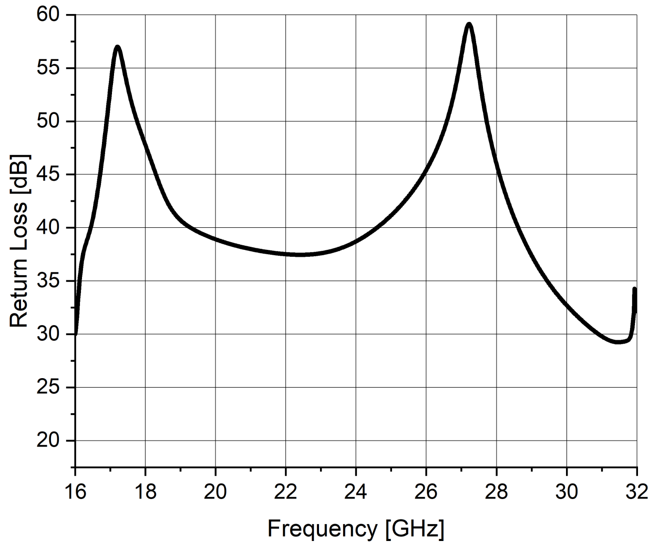

(b)

Figure 2.26: *(a) Vacuum Model and (b) Return Loss of the H-plane Bend.*

2.2.7 Adapters

Adapters are designed to convert the septum polarizer ports to standard waveguide dimensions. These waveguide structures are integrated at the input ports of both the Tx and Rx bands, symmetrically added to the LHCP and RHCP ports of the septum polarizers.

Rectangular waveguides with incrementally stepped dimensions are designed for adapters. A WR34 standard waveguide is used for the Rx band, while a WR51 standard waveguide is employed for the Tx band. Vacuum models of the two adapters are provided in Figure 2.27. Return and insertion loss graphs for the adapters are displayed in Figure 2.28. Both adapters exhibit greater than 30 dB return loss.

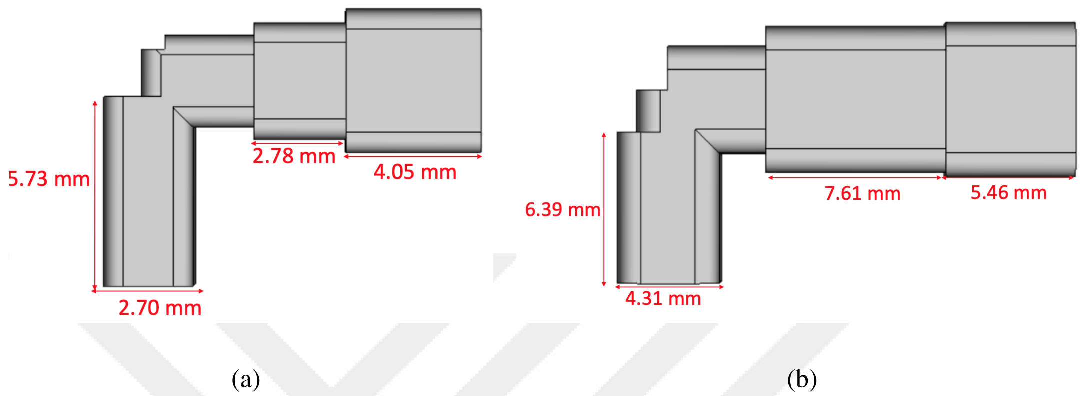

Figure 2.27: *Vacuum Models of (a) WR34 Rx and (b) WR51 Tx Septum Adapters.*

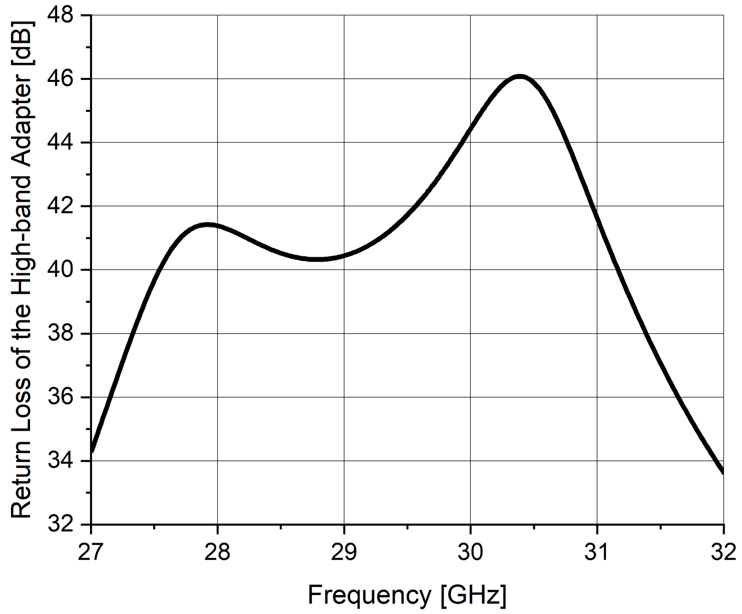

(a)

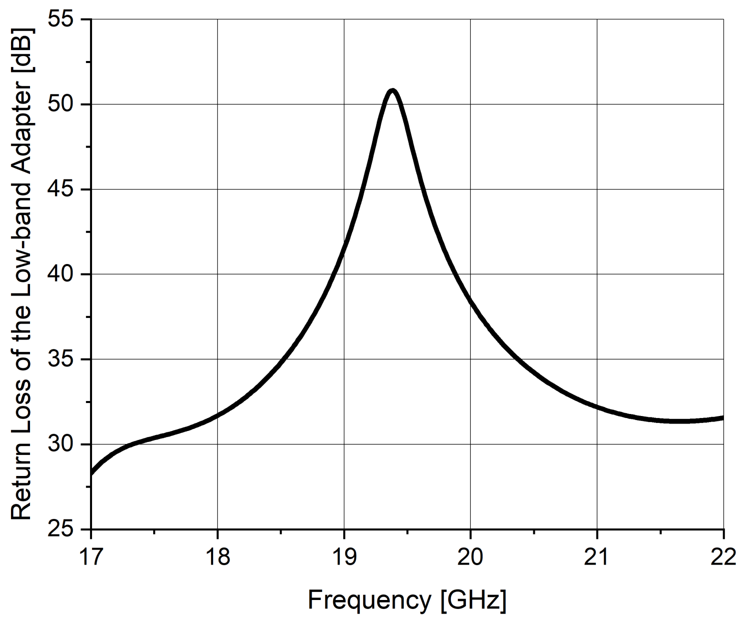

(b)

Figure 2.28: *Return Loss of (a) WR34 Rx and (b) WR51 Tx Septum Adapters.*

3. RESULTS OF THE INTEGRATED SYSTEM

As stated in Chapter 2, the components are designed individually and optimized through iterative refinements until the design targets are obtained. In this chapter, the integrated system and its simulation results are discussed. This design features four ports, two for the Tx band (Port 5 and Port 6) and two for the Rx band (Port 3 and Port 4). The results at these ports represent the key performance metrics: return loss, port-to-port isolation, Tx-Rx isolation, sidelobe level, and cross-polarization discrimination. Since this is a feed network and antenna design, the radiation patterns are also analyzed in detail. The results are sequentially illustrated and explained in independent sections. The entire system dimensions are smaller than 110 x 110 x 360 mm^3, and its Computer-Aided Design (CAD) design is presented in Figure 3.1.

In the beginning, the components of the feed network and antenna sections are integrated to analyze the performance of the complete system. During the integration process, several challenges are encountered. The first of these challenges results from the initial design and return loss of the six-port OMJ, which affected the in-band isolation. In order to achieve the target performance, namely 20 dB in both Tx and Rx bands, especially close to the edges of the frequency range in the extended Ka-band, numerous optimization iterations are carried out. Modifications are made to the six-port OMJ component and the circular-to-square waveguide interface to provide proper integration of the components. In the first six-port OMJ design, the circular waveguide is employed as Port 1; nevertheless, with the implemented design alterations, this circular waveguide is removed, and the component reached its final design. Another challenge is caused by the septum polarizer designed for the Tx band. When this septum polarizer is integrated into the feed network and simulated, the RF performance for both LHCP and RHCP, in terms of XPD, decreases to the target of 30 dB. The purpose of XPD is to observe the difference between the co-pol and cross-pol of the system [5]. This is due to the phase difference.

More precisely, this occurred in the Tx band between 19.7-21.2 GHz and in the Rx band between 30.5-31 GHz. In order to fulfill the target values, several optimizations are performed on this component, and the feed network is re-simulated after each optimization. This process is repeated many times to reach the final design.

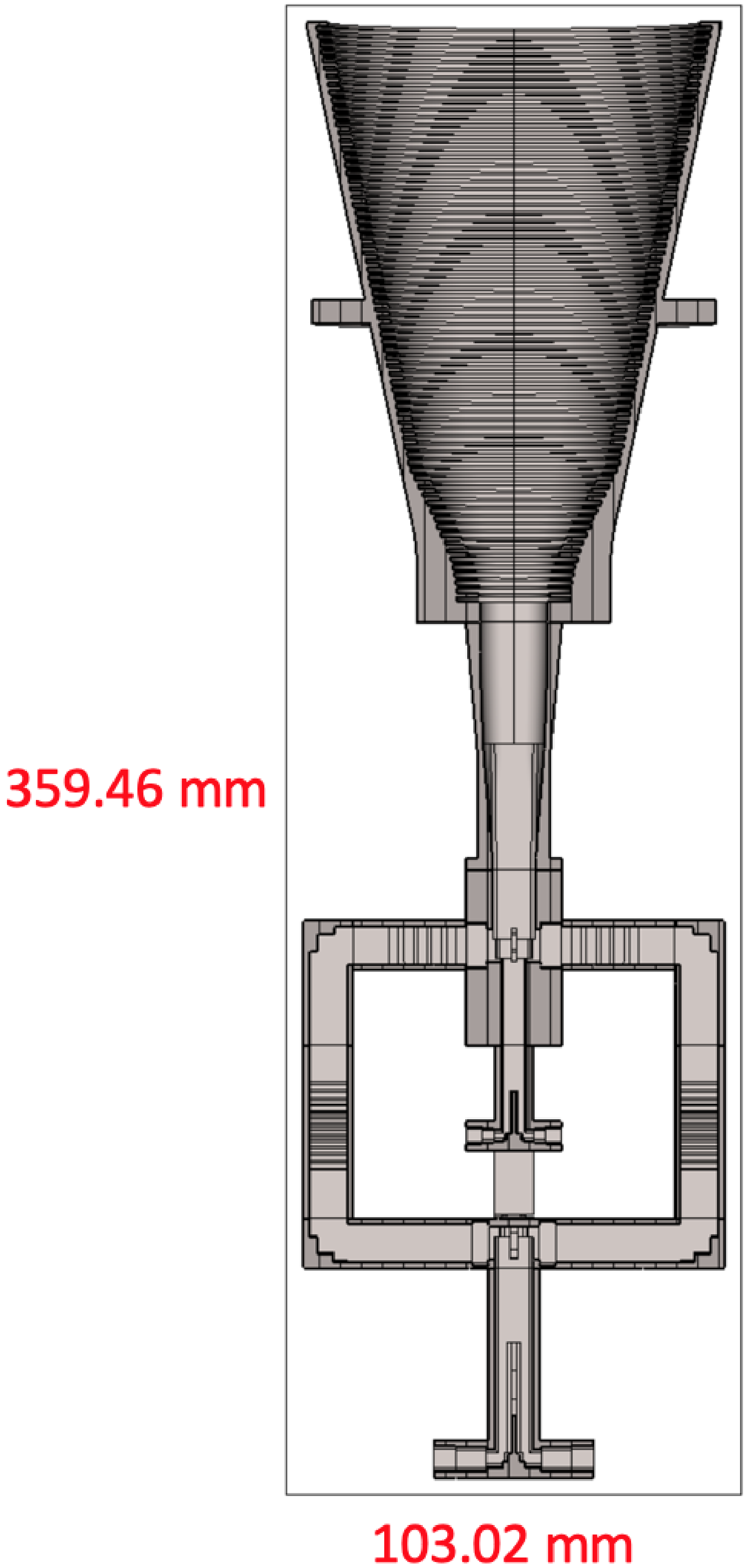

Figure 3.1: *CAD Model of the Complete System.*

3.1 Scattering Parameters

In this scattering parameters section, the integrated antenna-feed model is examined in terms of RF performance metrics, including return loss, port-to-port isolation, and Tx-Rx isolation.

Return loss is a crucial parameter quantifying how much of the signal is reflected back from the system. For both the Tx and Rx bands, the return loss is above 30 dB, namely, the system has low reflected power. The return loss of both the Tx and Rx bands are shown in Figure 3.2.

Preserving isolation across the whole system is significant to prevent signal leakage within the same bands, and it emerges as one of the key performance metrics. In both frequency bands, the in-band isolation exceeds 20 dB, demonstrating that there is minimal leakage between the adjacent ports. The in-band isolation of both the Tx and Rx bands are depicted in Figure 3.3.

The receiver operates over the frequency range of 27.5-31 GHz, and for proper system performance, signals within this band must be received while signals outside or near this range should be effectively rejected. This can be analyzed by examining the out-of-band isolation of the system. Although the system operates in dual-band, protecting and monitoring the receiver is particularly crucial, as inadequate isolation can result in performance degradations, including link failure, wideband noise interference, and reduced operational range. Since the system operates in dual-band, there must be adequate isolation between the Tx and Rx ports to prevent any signal leakage. As shown in Figure 3.4, the Tx-Rx isolation in the Tx band is above 80 dB up to 20.7 GHz, but decreases to 63 dB at 21.2 GHz, whereas in the Rx band, it exceeds 80 dB.

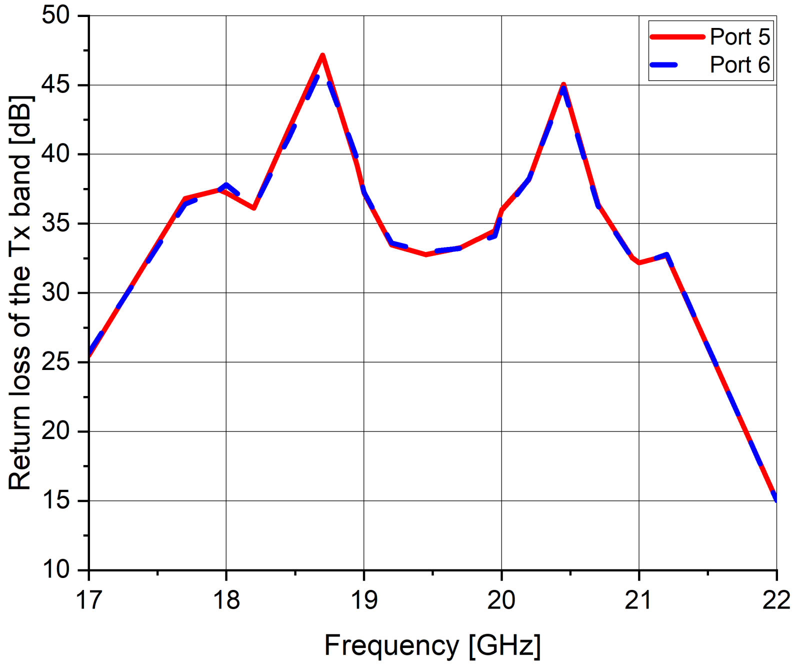

(a)

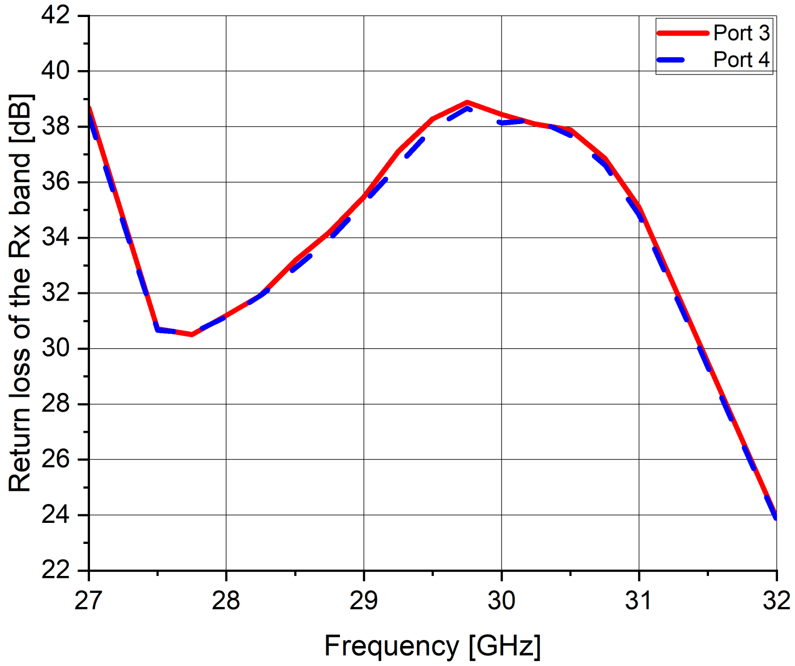

(b)

Figure 3.2: *(a) Return Loss of the Tx Band and (b) Return Loss of the Rx Band.*

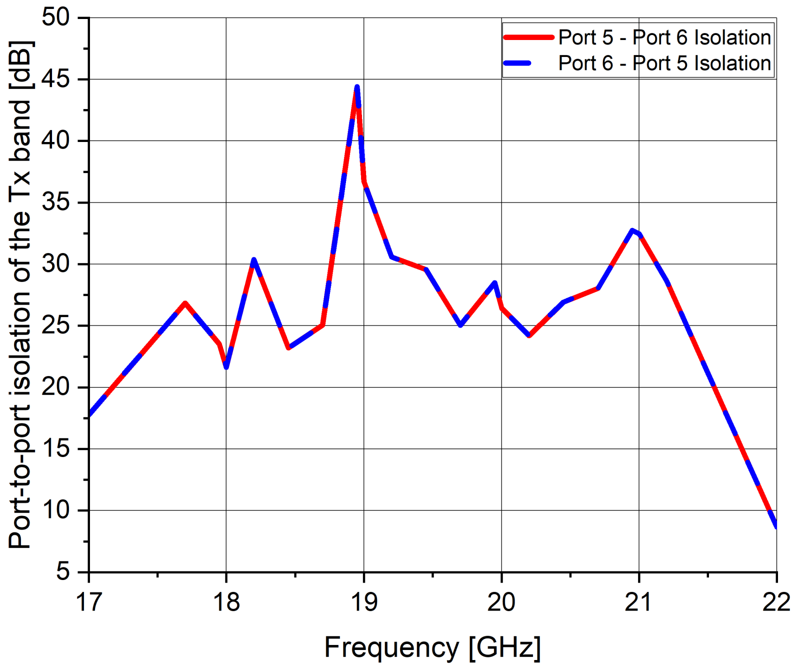

(a)

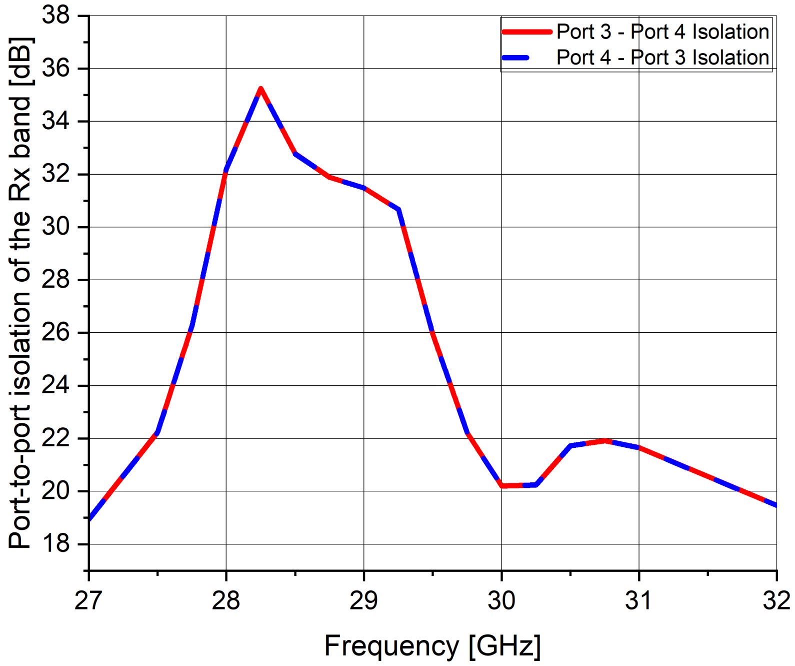

(b)

Figure 3.3: *(a) In-band Isolation of the Tx Band and (b) In-band Isolation of the Rx Band.*

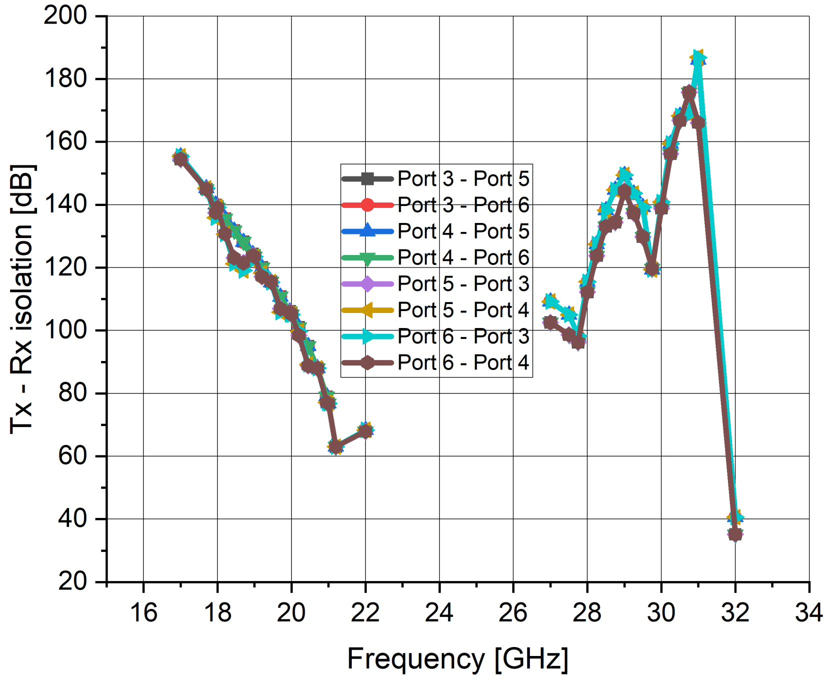

Figure 3.4: *Tx-Rx Isolation of the Integrated System.*

3.2 Radiation Patterns

In this section, the sidelobe level and XPD, which are the other performance metrics of the integrated antenna and feed network, are introduced. Subsequently, the radiation patterns of the overall system are analyzed for each port.

In addition to the sidelobe level, cross-polarization discrimination, and radiation pattern results, efficiency-related results, as well as the transmission coefficient, are also examined. Both radiation efficiency and total efficiency are analyzed using the linear values after integrating the entire structure.

By analyzing the amplitude levels of the sidelobes in the designed antenna, the level compared to the signal propagating in the main lobe is examined. The sidelobe level of the Tx band is below -31.3 dBc, which is illustrated in Figure 3.5. As shown in Figure 3.5, the sidelobe level of the Rx band is below -32 dBc.

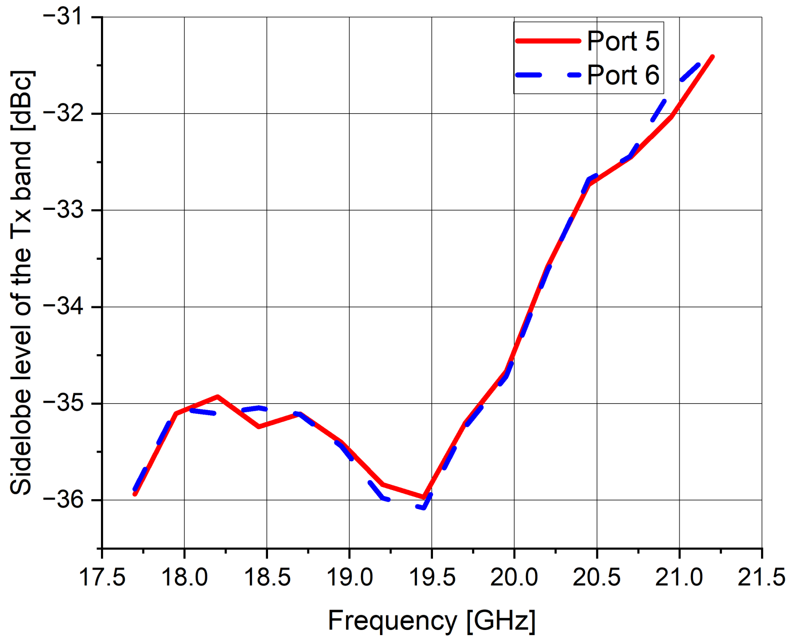

(a)

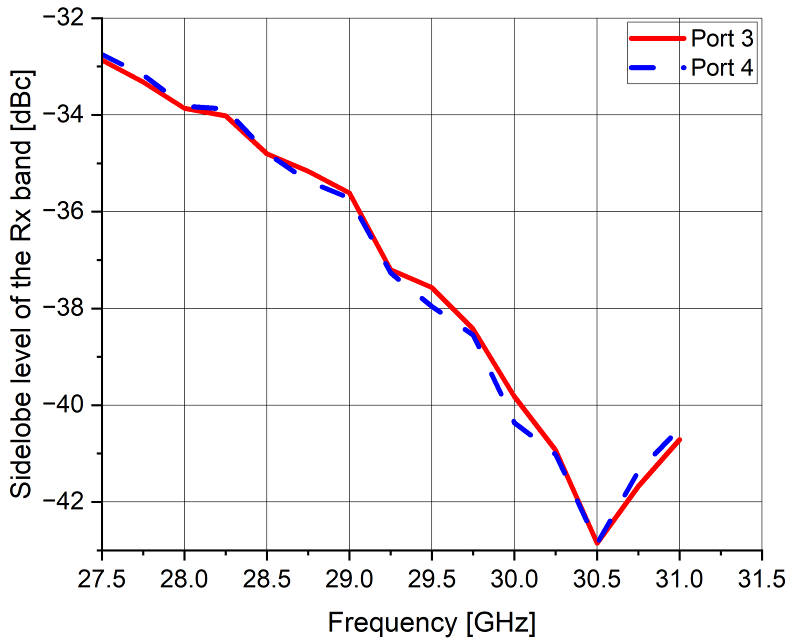

(b)

Figure 3.5: *(a) Sidelobe Level of the Tx Band and (b) Sidelobe Level of the Rx Band.*

Since a high-quality polarization is aimed for, cross-polarization discrimination plays a significant role in antenna design. The aim of XPD is to measure the difference between co-pol and cross-pol [5]. As can be observed in Figure 3.6, the cross-polarization discrimination exceeds 30 dB for both frequency bands. A cross-polarization discrimination exceeding 30 dB is not commonly observed in the literature, which also demonstrates good polarization purity and proper transmission of the signals.

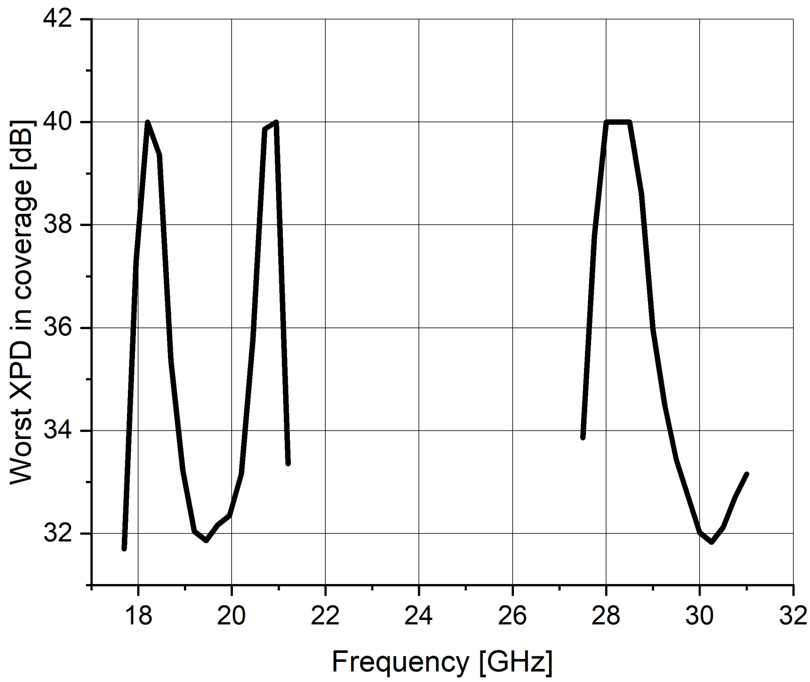

Figure 3.6: *Cross-polarization Discrimination of the Integrated System.*

As stated earlier, the results for the Rx band are examined using Port 3 and Port 4, while those for the Tx band are evaluated using Port 5 and Port 6. LHCP is generated at Port 3, whereas RHCP is generated at Port 4 in the Rx band. While RHCP is produced at Port 5, LHCP is produced at Port 6. The radiation pattern results are presented at the operating frequency with 250 MHz intervals. The co-polarized radiation patterns of Port 3 are depicted in Figure 3.7. The co-polarized radiation patterns of Port 4 are shown in Figure 3.9. The radiation pattern is nearly identical across the Rx band and circularly symmetric, yielding excellent cross-polarization discrimination exceeding 30 dB. The gain exceeds 26 dBi, with no noticeable sidelobe or back lobe variation. The cross-polarized radiation patterns of Port 3 are demonstrated in Figure 3.8. In Figure 3.10, the cross-polarized radiation patterns of Port 4 can be observed.

Likewise, the co-polarized radiation patterns of Port 5 indicate the same characteristics, with a gain exceeding 24 dBi, with no perceptible sidelobe or back lobe change as can be observed in Figure 3.11. Additionally, the co-polarized radiation patterns of Port 6 can be seen in Figure 3.13. The cross-polarized radiation patterns resulting from Port 5 are shown in Figure 3.12. The result corresponding to Port 6 operating within the Tx band is illustrated in Figure 3.14.

Radiation efficiency shows the fraction of the power accepted by the antenna that is converted into radiated power and is affected by the losses of the conductor and the tolerances of the corrugated horn antenna. It is used to analyze antenna performance in isolation. Return loss is not included in the calculation of radiation efficiency. The radiation efficiency of Port 3 and Port 4 is approximately 0.96, while the values for Port 5 and Port 6 are close to 0. This reduction in efficiency for Tx ports is due to the integration of the entire structure and the resulting loss of conductors in the aluminum components. These results exhibit the high performance of the system.

Total efficiency represents the fraction of the input power applied to the antenna that is actually radiated. Unlike radiation efficiency, return loss is included in its calculation and accounts for losses in both the antenna and the feed network. It is used to examine the real efficiency of the entire system. The total efficiency of Port 3 and Port 4 is approximately 0.958, while the values for Port 5 and Port 6 are close to 0.

In this system, the transmission coefficient indicates the ratio of power transmitted from one port to another. When evaluated on a linear scale, the total efficiency of a port is closely correlated and consistent with its transmission coefficient. The total efficiency results are also calculated using the logarithmic formula to analyze losses in dB, showing that the loss is below -0.2 dB, namely, the structure exhibits minimal power loss.

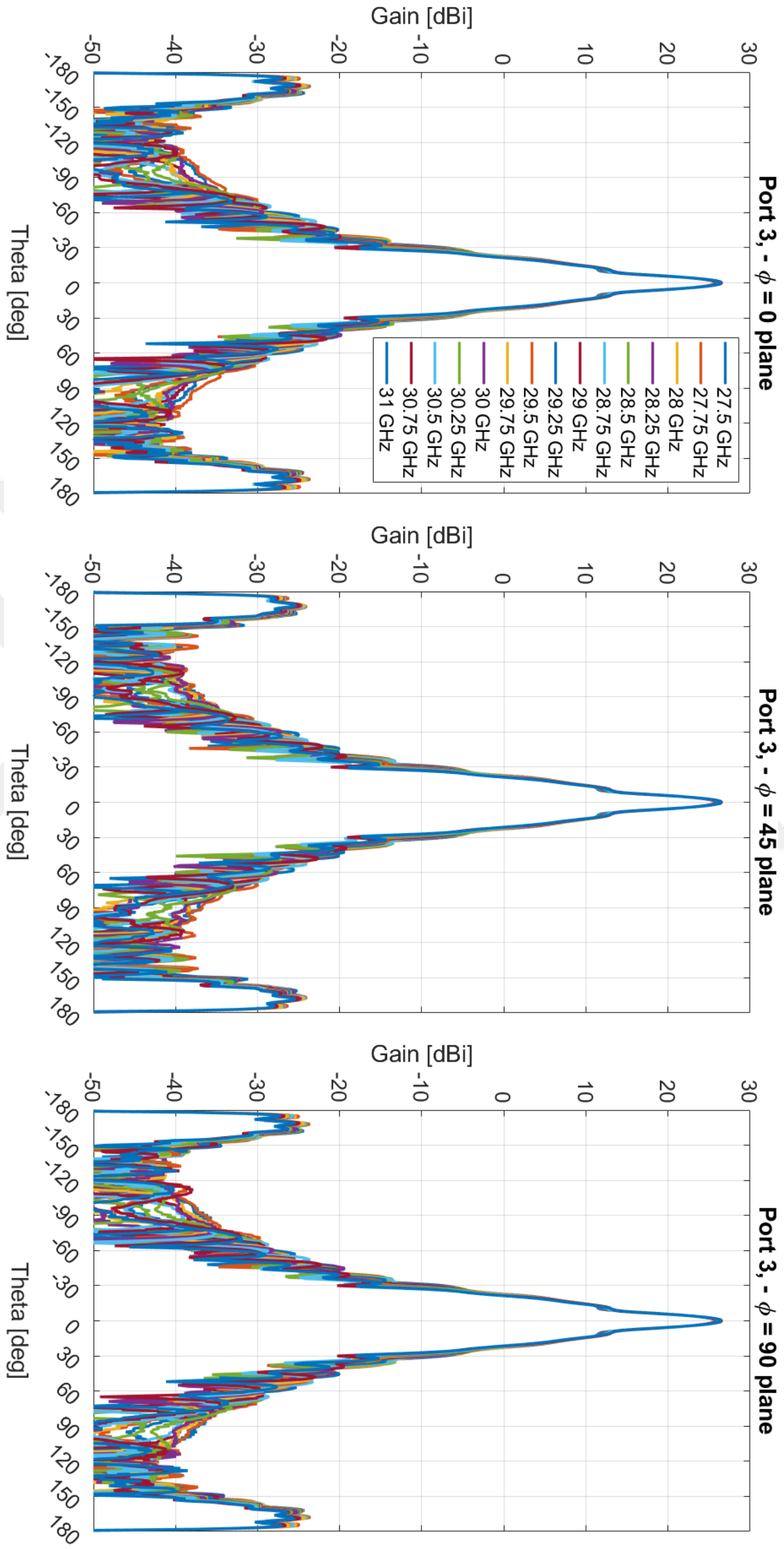

Figure 3.7: *Rx Co-polarized (LHCP) Radiation Patterns at Port 3.*

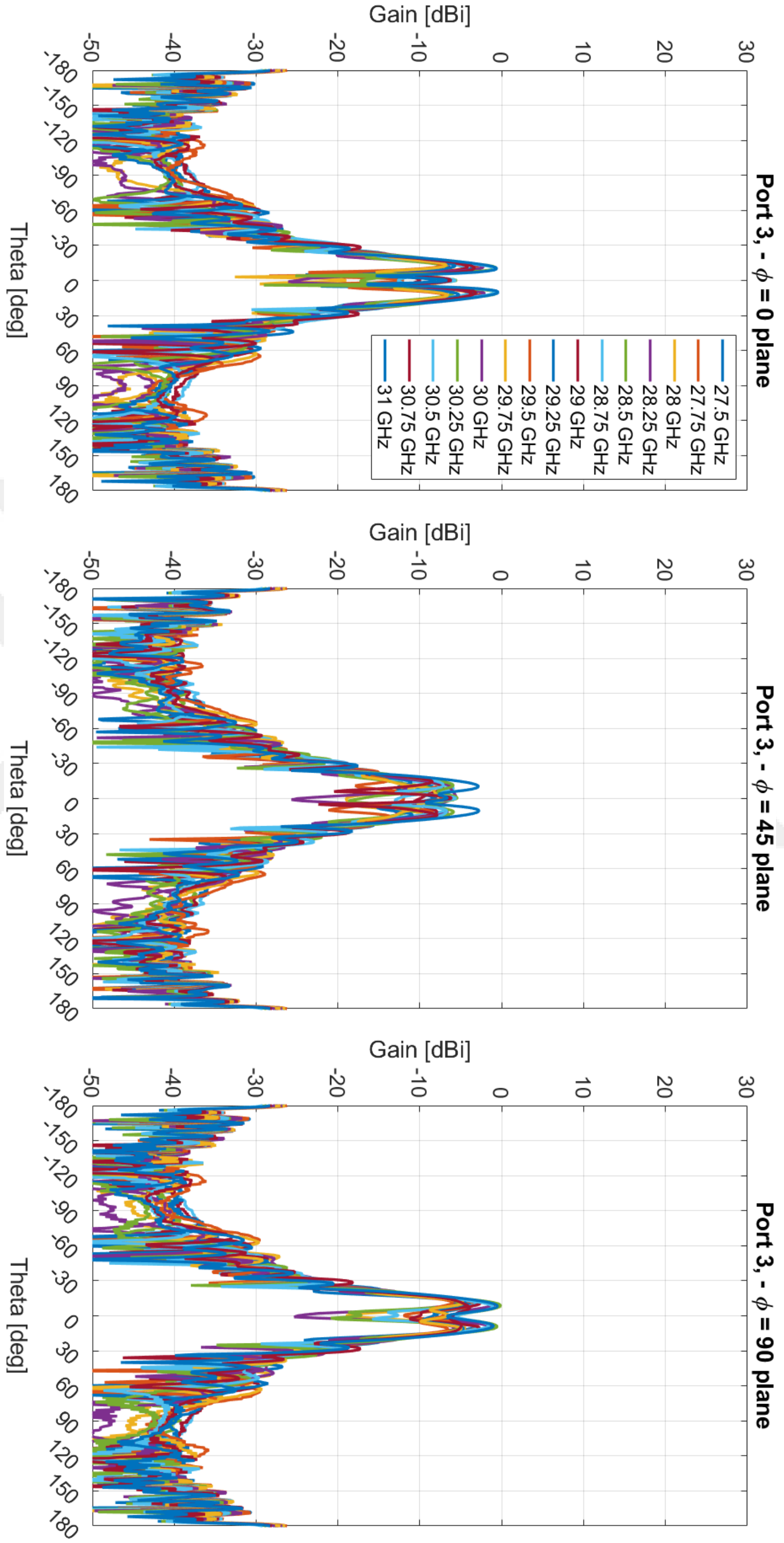

Figure 3.8: *Rx Cross-polarized (RHCP) Radiation Patterns at Port 3.*

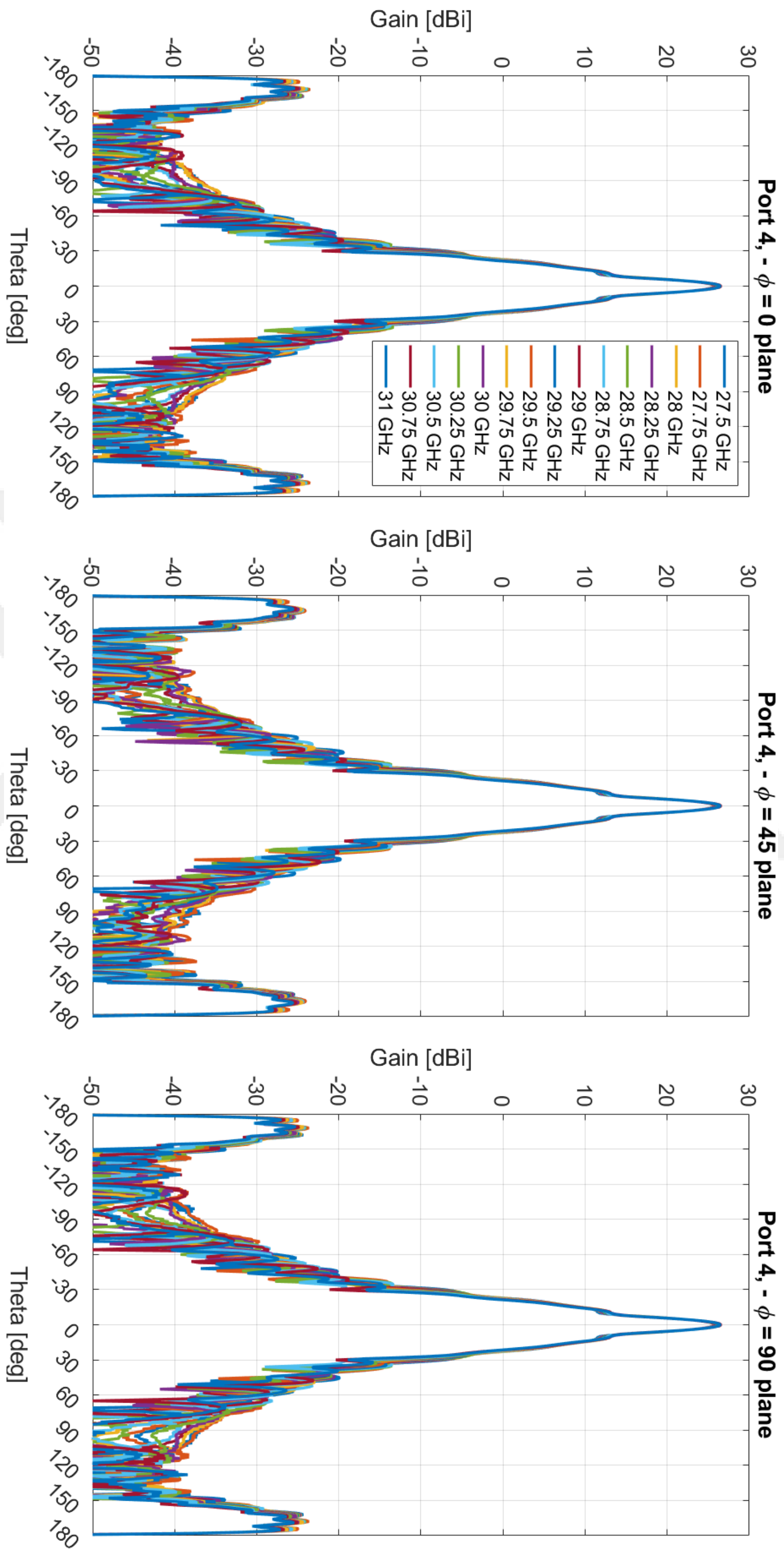

Figure 3.9: *Rx Co-polarized (RHCP) Radiation Patterns at Port 4.*

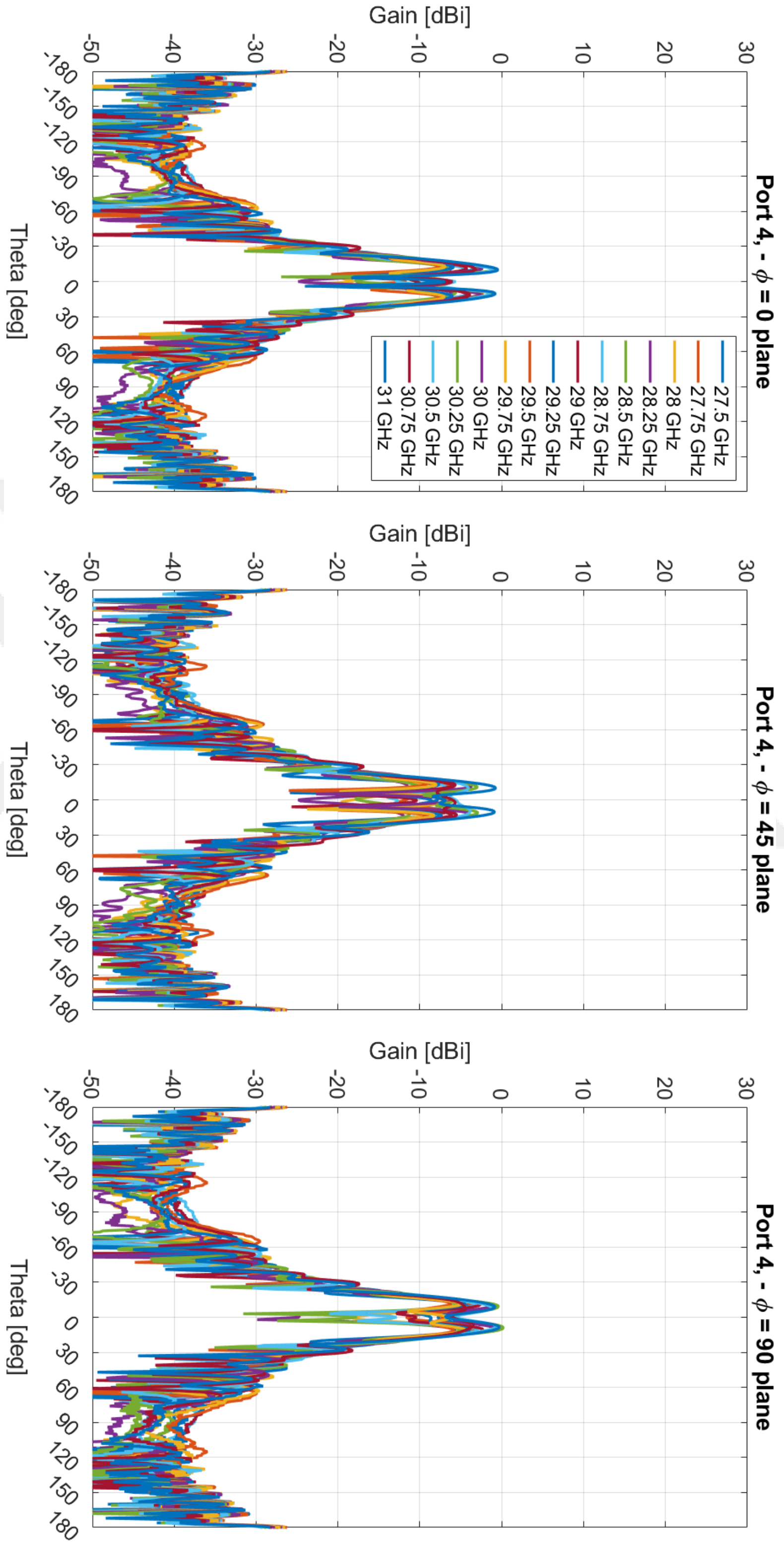

Figure 3.10: *Rx Cross-polarized (LHCP) Radiation Patterns at Port 4.*

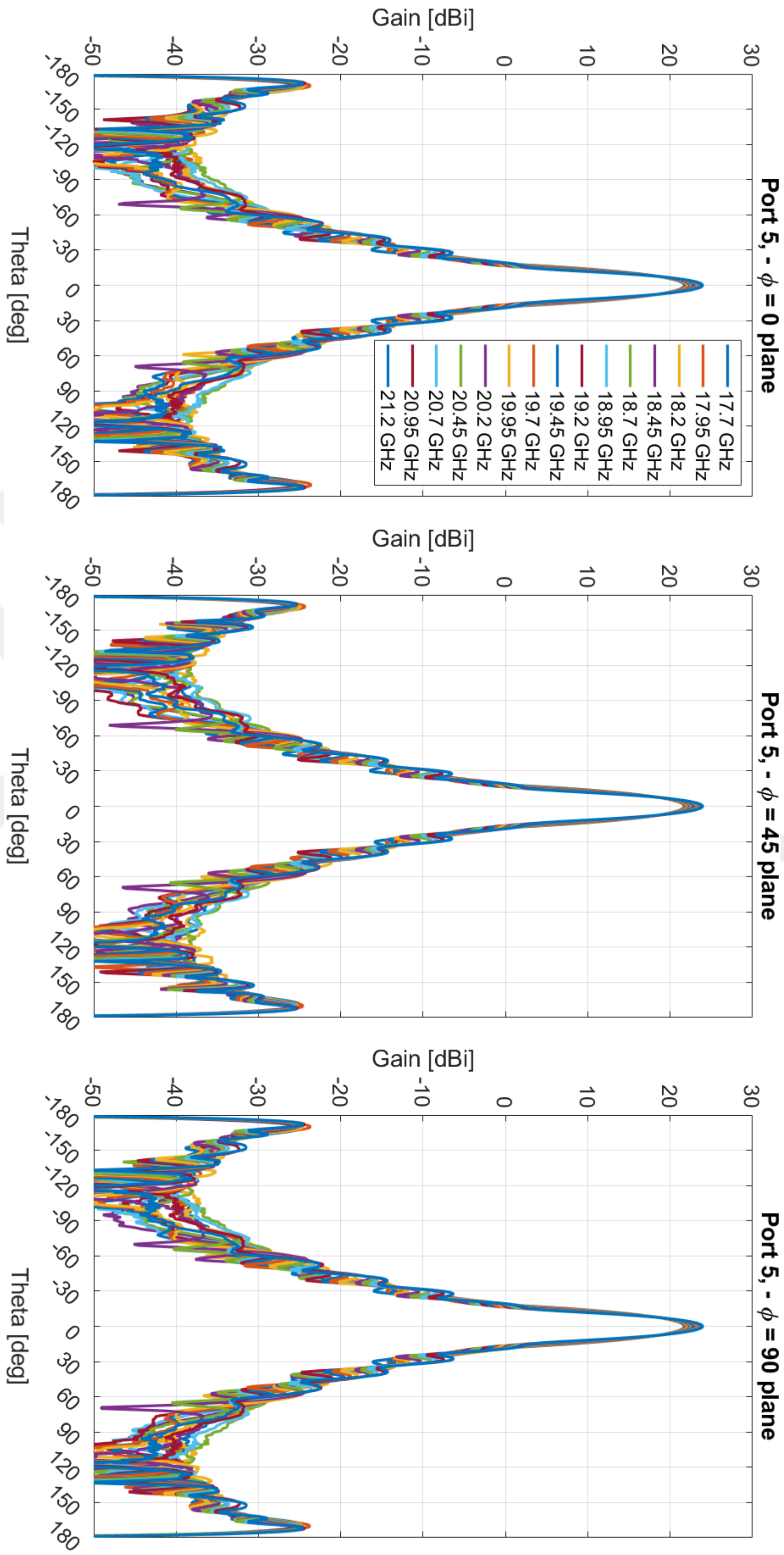

Figure 3.11: *Tx Co-polarized (RHCP) Radiation Patterns at Port 5.*

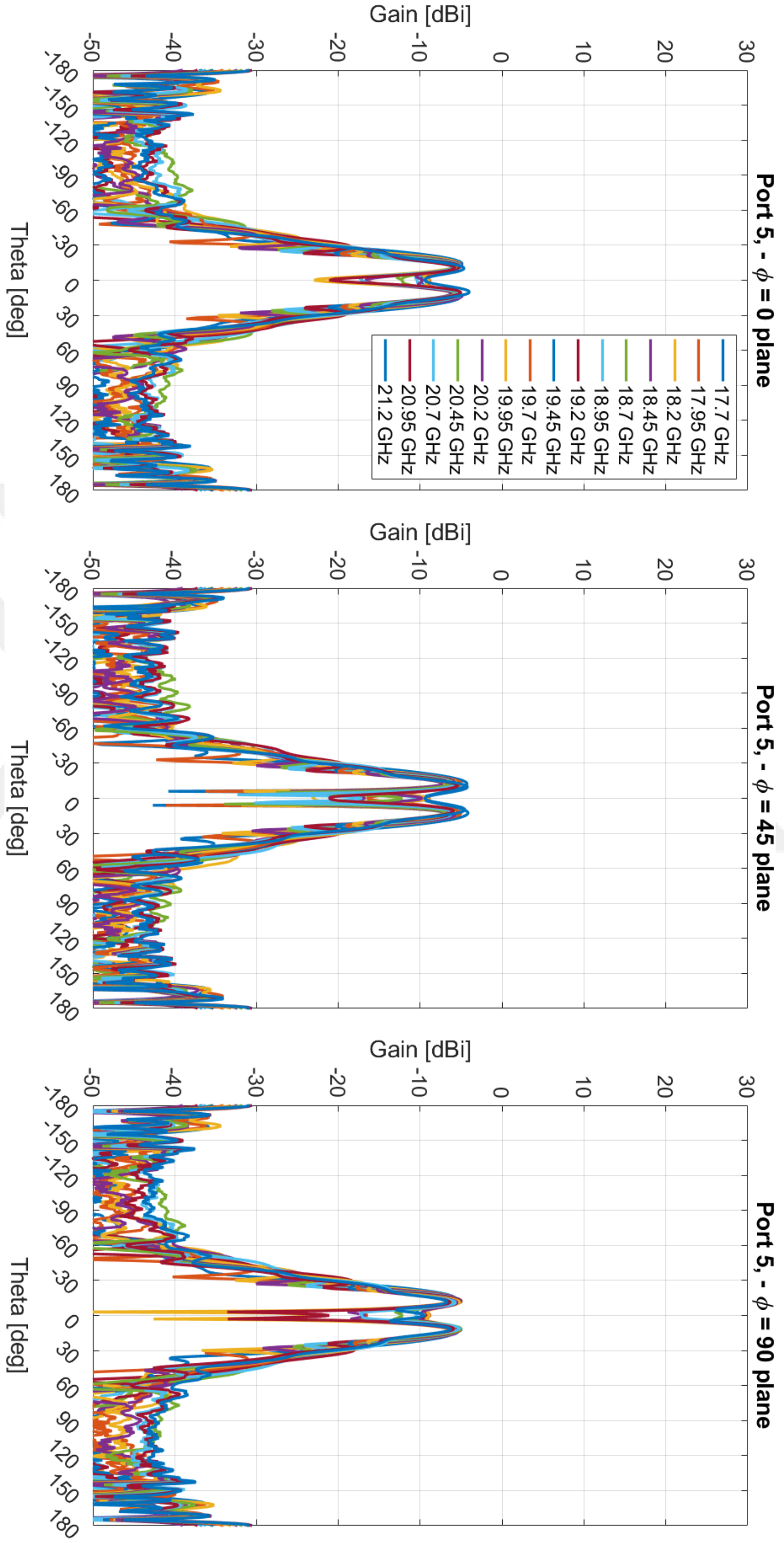

Figure 3.12: *Tx Cross-polarized (LHCP) Radiation Patterns at Port 5.*

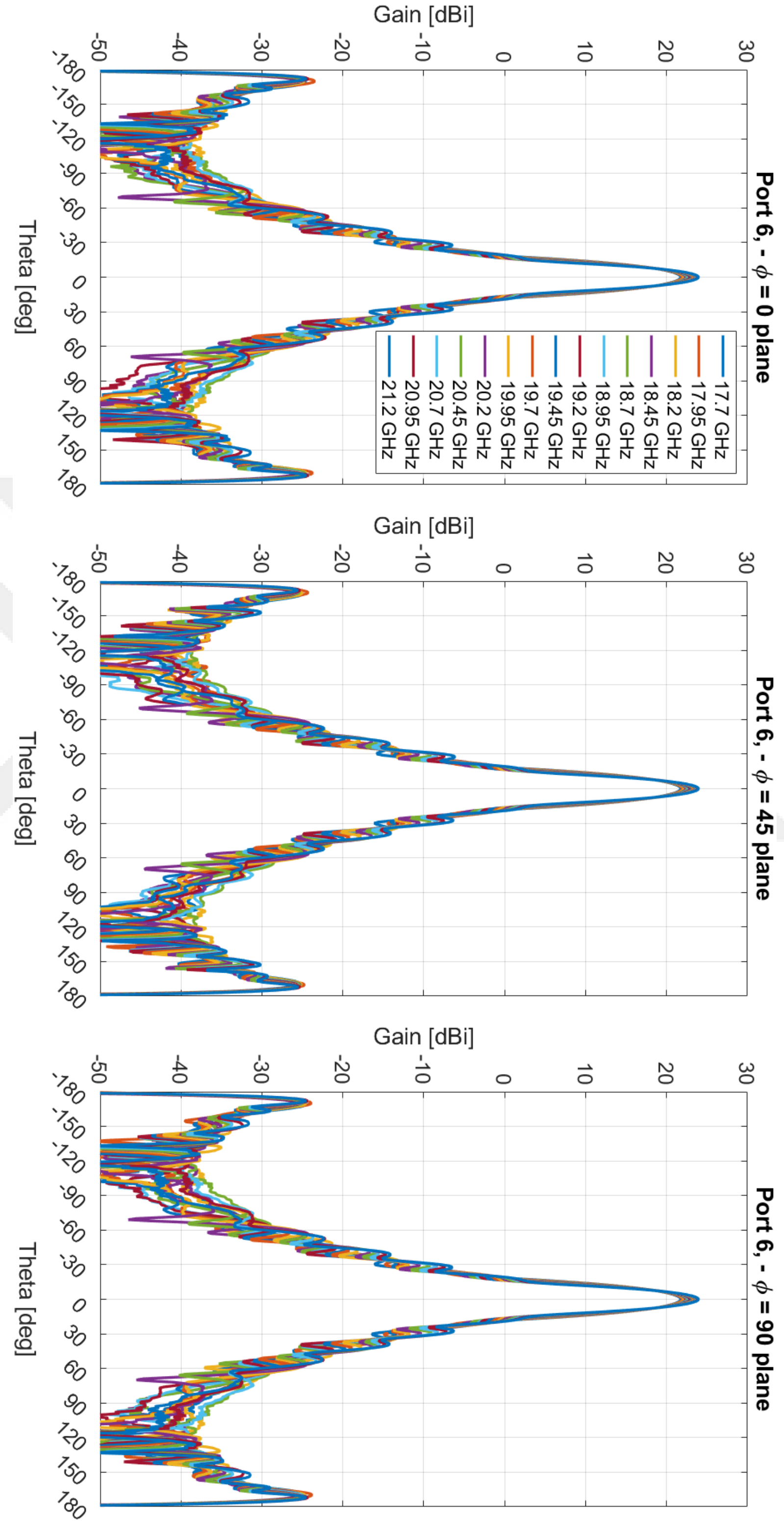

Figure 3.13: *Tx Co-polarized (LHCP) Radiation Patterns at Port 6.*

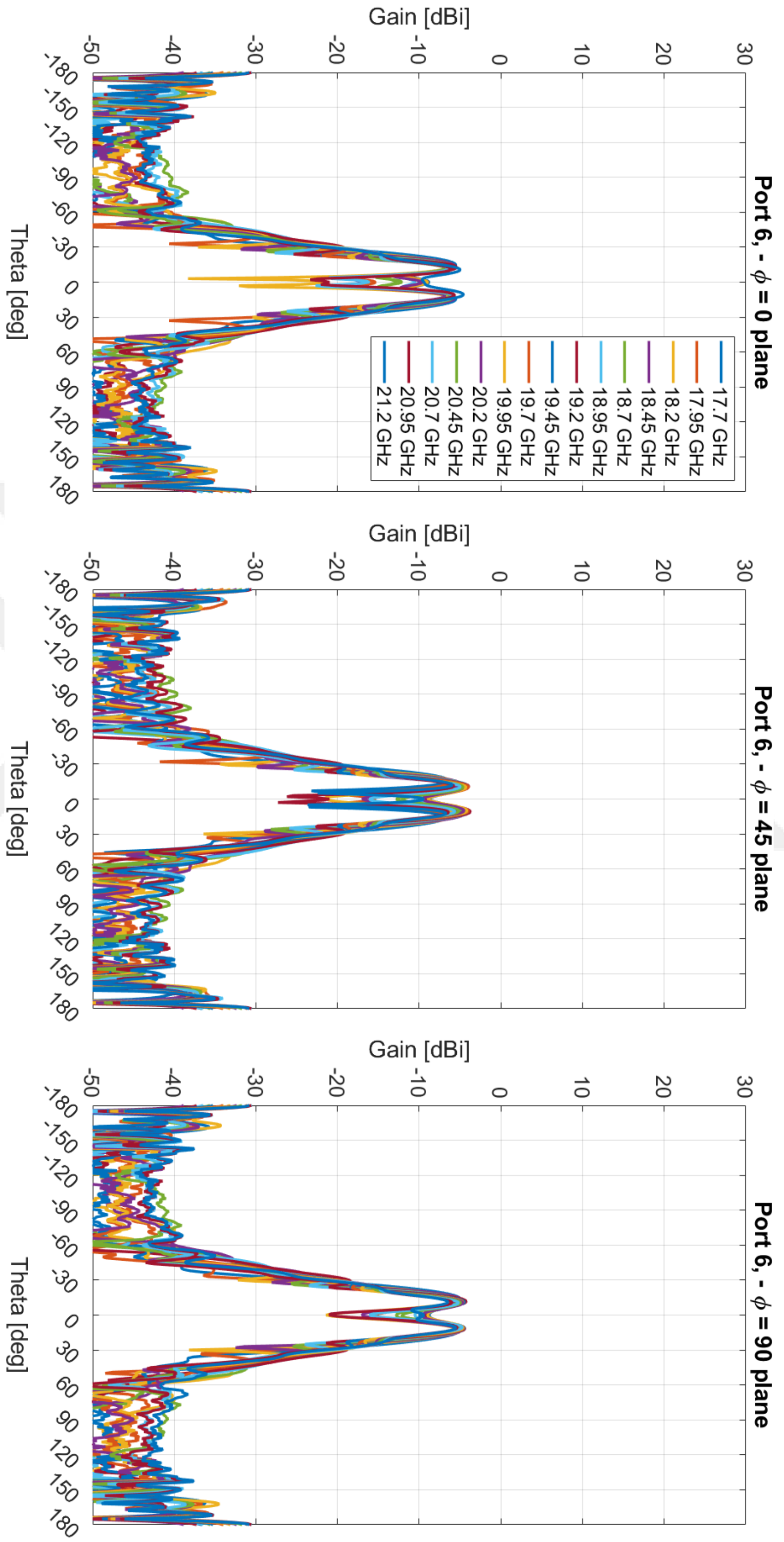

Figure 3.14: *Tx Cross-polarized (RHCP) Radiation Patterns at Port 6.*

4. CONCLUSIONS

A compact, dual-circular Ka-band SATCOM payload with excellent electrical performance is introduced in this thesis. Corrugated horn antenna, radial mode converter, circular-to-square waveguide transition, a six-port OMJ, two different waveguide low-pass filters, two different H-plane bends, a five-port OMJ, septum polarizers, and adapters are designed for small geostationary satellite applications. The specified components are first designed individually, then optimized, and finally combined and analyzed to determine their ability to meet the desired performance targets. Consequently, an antenna-feed model operating in the extended Ka-band and enabling dual circular polarization is developed for use in SATCOM applications.

Critical parameters for this design are operating frequencies, minimum and maximum gain, sidelobe level, polarization, cross-polarization discrimination, port-to-port isolation, Tx-Rx isolation, return loss, interface, and dimension. In Table 4.1, the RF performance is compared with the design specifications. When analyzing Table 4.1, it can be observed that the parameter values achieved in the design differ only negligibly from the defined target values. WR34 standard waveguide is employed for the receiver frequency band, whereas WR51 standard waveguide is used for the transmitter frequency band. The antenna features a compact footprint of 110 x 110 x 360 mm^3. The radiation pattern remains practically identical across two operating frequency bands. The radiation pattern is circularly symmetric, achieving excellent cross-polarization discrimination higher than 30 dB. The results represent that a compact structure operating within this dual frequency range and having this level of performance is a crucial contribution to the field. The design has been finalized in a form suitable for fabrication, along with simulation results. Radii and blends have been integrated into the components.

During the design process of the components employed in this thesis, the potential structural implementations of each component are observed. Hence, the design approach

Table 4.1: *Design Specifications and the RF Performance Results.*

Parameter	Specifications	Simulation Results
Operating Frequency	17.7-21.2 GHz for Tx, 27.5-31 GHz for Rx	17.7-21.2 for Tx, 27.5-31 GHz for Rx
Polarization	RHCP & LHCP	RHCP & LHCP
Minimum Gain	21 dBi for Tx, 23.3 dBi for Rx	21.1 dBi for Tx, 23.8 dBi for Rx
Maximum Gain	23.3 dBi for Tx, 26.8 dBi for Rx	23.9 dBi for Tx, 26.5 dBi for Rx
Sidelobe Level	< -30 dBc	< -31.3 dBc
Cross-Polarization Discrimination	≥ 30 dB (over EOC)	≥ 30 dB (over EOC)
Return Loss	> 30 dB (for each port)	> 30 dB (for each port)
Port-to-port Isolation	> 20 dB (over EOC)	> 20 dB (over EOC)
Tx-Rx Isolation	> 80 dB	> 63 dB

is guided not by operating frequency alone but by analyzing the design and performance characteristics of similar components examined in previous works. By comparing the overall system with existing state-of-the-art designs in Table 4.2, the analysis of the contributions and promising advancements presented by this thesis is conducted.

When reviewing the studies conducted in this field, one of the first comparable systems encountered a similar feed network structure operating in the same frequency range, even though the Tx and Rx bands are switched. Its RF performance also shows certain similarities, for instance, the return loss exceeding 30 dB when the corrugated horn antenna is integrated into the system [7]. Nevertheless, there is an important difference in terms of Tx-Rx isolation and port-to-port isolation. In this thesis, the Tx-Rx isolation is over 63 dB, whereas the port-to-port isolation is better than 20 dB.

In another feed network design, the operating frequency range is the same band but over a narrower range, especially 19.25-20.75 GHz and 27-29 GHz, which shows structural differences compared to the design introduced in this thesis [10]. Both its return loss, port-to-port isolation, and cross-polarization discrimination are higher than that achieved in the current design.

In the design by Hong et al. [12], the system operates in 17.7-20.2 GHz for the Tx band and 27.5-30 GHz for the Rx band. It includes a horn, a Tx/Rx polarizer network, and OMJ, including a diplexer. In addition, this design supports dual circular polarization, and its return loss is over 25 dB, and its port-to-port isolation is above 21 dB, with the measurement and simulation results being similar. When compared to the design introduced in this thesis, the performance remains at a lower level.

In Gong et al. [14], the extended Ka-band is not covered, but it provides dual circular polarization. Return loss is better than 30 dB, and port-to-port isolation exceeds 19 dB. This again emphasizes that the extended frequency ranges and the achieved performance in this thesis present a distinct improvement within this field.

Table 4.2: *Comparison of This Design with State-of-the-art Dual Circular Polarization Designs.*

Parameter	**[7]**	**[10]**	**[12]**	**[14]**	**This work**
Frequency [GHz]	17.7-21.2, 27.5-31	19.25-20.75, 27-29	17.7-20.2, 27.5-30	17.7-20.2, 27.5-30	17.7-21.2, 27.5-31
XPD	N/A	$>$ 35 dB	N/A	N/A	$\geq$ 30 dB
Return Loss	$>$ 30 dB	$>$ 30 dB	$>$ 25 dB	$>$ 30 dB	$>$ 30 dB
Port-to-port Iso.	$>$ 18 dB	$>$ 22 dB	$>$ 21 dB	$>$ 19 dB	$>$ 20 dB
Tx-Rx Iso.	$>$ 100 dB	N/A	$>$ 55 dB	$>$ 75 dB	$>$ 63 dB

A revision can be made to the 13-section waveguide low-pass filter designs in order to increase the out-of-band isolation in both the Tx and the Rx bands as required. Therefore, a Tx-Rx isolation exceeding 80 dB, or even around 100 dB, can be achieved in both bands, similar to the literature. This modification does not necessitate this structure expanding and is, in fact, not a significant alteration.

As future work, it could be proposed to compare simulation outcomes with the fabricated results, to further compact the integrated antenna-feed model, to alter the design to function across a wider Ka-band frequency band, to integrate two separate frequency bands, for example, X and K, within the same structure, to enable their use in various space applications, or to implement advanced materials and manufacturing techniques for this design [26, 27, 28].

In conclusion, in most studies described in the literature, radial mode converters are not used in such a system, or a smaller number of low-pass filters is used, which can be considered a novel aspect. The design presented in this thesis improves previous works by providing a dual circularly polarized and dual-band system operating over the same frequency range, while extending to the Ka-band. Moreover, by achieving a good performance level, the system accomplishes a cross-polarization discrimination exceeding 30 dB, representing a crucial contribution to the literature. As a result, a compact and good performance design suitable for SATCOM applications has been realized.

REFERENCES

[1] P. Wang, J. Zhang, X. Zhang, Z. Yan, B. G. Evans, and W. Wang, "Convergence of satellite and terrestrial networks: A comprehensive survey," *IEEE Access*, vol. 8, pp. 5550–5588, 2020.

[2] B. Li, Z. Fei, C. Zhou, and Y. Zhang, "Physical-layer security in space information networks: A survey," *IEEE Internet of Things Journal*, vol. 7, no. 1, pp. 33–52, 2020.

[3] J. Rainbow, "How smaller satellites are reshaping the geostationary orbit market," May 2025. [Accessed May-2025].

[4] J. Christensen, "Itu regulations for ka-band satellite networks," Oct. 2012. [Accessed October-2024].

[5] P. Kildal, *Foundations of Antenna Engineering: A Unified Approach for Line-of-Sight and Multipath*. Artech House, 2015.

[6] P. J. B. Clarricoats and A. D. Olver, *Corrugated Horns for Microwave Antennas*. IET, 1984.

[7] S. Yang, M. Cai, Z. Yan, and T. Zhangi, "A dual band/dual polarization compact feed chain for satelitte communication applications," in *International Symposium on Antennas and Propagation (ISAP)*, pp. 1–3, 2019.

[8] S.-G. Park, H. Lee, and Y.-H. Kim, "A turnstile junction waveguide orthomode transducer for the simultaneous dual polarization radar," in *2009 Asia Pacific Microwave Conference*, pp. 135–138, 2009.

[9] J. M. Pandya, K. Sood, and Pujara, "Novel slot-coupled broadband waveguide junction for orthomode transducer using mirrored semi-profiled section," *Microwave and Optical Technology Letters*, vol. 60, pp. 2309–2314, Aug. 2018.

[10] G. Addamo, M. Lumia, F. Clignano, F. Paonessa, G. Virone, D. Manfredi, L. Iuliano, and P. O.A., "3d printing of a monolithic k/ka-band dual-circular polarization antenna-feeding network," *IEEE Access*, vol. 9, pp. 88243–88255, 2021.

[11] D. Garcia, J. Cabrera, and M. M. Ruiz, "High performance of dual band/dual polarization compact omt," in *IEEE-APS Topical Conference on Antennas and Propagation in Wireless Communications (APWC)*, pp. 703–706, 2013.

[12] U. P. Hong, S. Stirland, R. Gehring, C. Hartwanger, and H. Wolf, "A dual circular combined k/ka-band user and gateway feed chain for multi beam satellite antennas," in *32nd ESA Antenna Workshop*, 2010.

[13] M. Chen and G. Tsandoulas, "A wide-band square-waveguide array polarizer," *IEEE Transactions on Antennas and Propagation*, vol. 21, pp. 389–391, May. 1973.

[14] J.-G. Gong, Q. Li, M.-T. Zhang, J. Hou, Y. Wang, and Z. Xu, "A wideband dual circular polarization feed chain for satellite antennas at k/ka bands," in *2017 Progress In Electromagnetics Research Symposium - Spring (PIERS)*, pp. 222–226, 2017.

[15] J. Kot, C. Granet, I. Davis, K. Verran, and T. Mellor, "Dual-band feed systems for SATCOM antenna applications," in *Asia-Pacific Microwave Conference*, pp. 662–665, 2011.

[16] U.S. Department of Commerce, National Telecommunications and Information Administration, "U.s. frequency allocation chart as of october 2003," Oct. 2003. [Accessed: October-2003].

[17] H. Manigilla, P. K. Mishra, R. R., P. S., P. V.B, and R. V. Nadagouda, "Broadband k/ka band dual-linear/dual-circular polarized feed design for satellite payload testing in compact antenna test ranges," in *2025 IEEE Space, Aerospace and Defence Conference (SPACE)*, pp. 1–6, 2025.

[18] A. D. Olver, P. J. B. Clarricoats, L. Shafai, and A. Kishk, *Microwave Horns and Feeds*. IET, 1994.

[19] C. Granet and G. L. James, "Design of corrugated horns: a primer," *IEEE Antennas and Propagation Magazine*, vol. 47, pp. 76–84, Apr. 2005.

[20] G. James, "Design of wide-band compact corrugated horns," *IEEE Transactions on Antennas and Propagation*, vol. 32, no. 10, pp. 1134–1138, 1984.

[21] B. Thomas, G. James, and K. Greene, "Design of wide-band corrugated conical horns for cassegrain antennas," *IEEE Transactions on Antennas and Propagation*, vol. 34, no. 6, pp. 750–757, 1986.

[22] C. A. Balanis, *Advanced Engineering Electromagnetics*. John Wiley & Sons, 2012.

[23] R. J. Cameron, C. M. Kudsia, and R. R. Mansour, *Microwave Filters for Communication Systems: Fundamentals, Design and Applications*. John Wiley & Sons, 2007.

[24] F. Teberio, I. Arnedo, J. M. Percaz, I. Arregui, T. Lopetegi, and M. A. G. Laso, "Accurate design of corrugated waveguide low-pass filters using exclusively closed-form expressions," in *2017 47th European Microwave Conference (EuMC)*, pp. 632–635, 2017.

[25] F. F. Dubrovka, S. I. Piltyay, R. R. Dubrovka, M. M. Lytvyn, and S. M. Lytvyn, "Optimal designs of x-band waveguide stepped-thickness septum polarizer," *Radioelectronics and Communications Systems*, vol. 64, no. 9, pp. 494–500, 2021.

[26] C. Lee-Yow, P. Venezia, and S. Rao, "High performance antenna feed systems for satellite communications," in *2023 IEEE Wireless Antenna and Microwave Symposium (WAMS)*, pp. 1–5, 2023.

[27] J. Teniente, I. Gómez-López, R. Caballero-Nagore, G. Crespo-López, and A. Martínez-Agoües, "Quad band x/ka horn antenna and feed chain designs," in *2017 11th European Conference on Antennas and Propagation (EUCAP)*, pp. 3432–3436, 2017.

[28] W. Zhang, H. Zhou, B. Falkner, S. Singh, A. Mehta, S. S. Milward, D. Butcher, N. Lavery, and S. G. Brown, "3d metal printed polarization reconfigurable horn antenna with solid meshed structures: Future works for satcom applications," in *2020 IEEE International Symposium on Antennas and Propagation and North American Radio Science Meeting*, pp. 1501–1502, 2020.